

Lawrence Berkeley National Laboratory

Recent Work

Title

ANTIPROTON ANNIHILATION AT REST IN DEUTERIUM

Permalink

<https://escholarship.org/uc/item/54m1d2fm>

Author

Kojoian, Gabriel.

Publication Date

1966-02-21

University of California
Ernest O. Lawrence
Radiation Laboratory

ANTIPROTON ANNIHILATION AT REST IN DEUTERIUM

TWO-WEEK LOAN COPY

*This is a Library Circulating Copy
which may be borrowed for two weeks.
For a personal retention copy, call
Tech. Info. Division, Ext. 5545*

Berkeley, California

DISCLAIMER

This document was prepared as an account of work sponsored by the United States Government. While this document is believed to contain correct information, neither the United States Government nor any agency thereof, nor the Regents of the University of California, nor any of their employees, makes any warranty, express or implied, or assumes any legal responsibility for the accuracy, completeness, or usefulness of any information, apparatus, product, or process disclosed, or represents that its use would not infringe privately owned rights. Reference herein to any specific commercial product, process, or service by its trade name, trademark, manufacturer, or otherwise, does not necessarily constitute or imply its endorsement, recommendation, or favoring by the United States Government or any agency thereof, or the Regents of the University of California. The views and opinions of authors expressed herein do not necessarily state or reflect those of the United States Government or any agency thereof or the Regents of the University of California.

Research and Development

UCRL-16717

UNIVERSITY OF CALIFORNIA
Lawrence Radiation Laboratory
Berkeley, California

AEC Contract No. W-7405-eng-48

ANTIPROTON ANNIHILATION AT REST IN DEUTERIUM

Gabriel Kojoian

Ph. D. Thesis

February 21, 1966

Contents

Abstract	v
I. Introduction	1
II. Experimental Procedure	3
A. Beam	3
B. Scanning	3
C. Sketching and Measuring	5
D. Data Processing.	5
1. Event Reconstruction.	5
2. Kinematical Fitting	7
III. Analysis of Data	9
A. Identification of Events at Rest	9
B. Analysis of Events	9
C. Analysis of Five-Prong Annihilations	15
IV. Discussion of Results.	22
A. Pion Multiplicity Distribution	22
B. Pion Momentum Distribution	25
C. Pion-Pion Correlations	25
D. Multi-Pion Events.	33
E. Five-Prong Annihilations and Selection Rules	36
F. Proton Momentum Distribution	37
1. Two-Body Antiproton Interactions.	37
2. Final-State Interactions.	45
3. Three-Body Antiproton Interactions.	51
G. Strange Particle Production.	61A

Acknowledgements 68

Appendices 69

 A. Predictions of the Statistical Model 69

 B. Derivation of Momentum Space Distribution of a
 Hulthén Simulated Hard Core Function. 71

 C. Derivation of Momentum Space Distribution of
 Three-Body Wave Functions 75

References 82

V

Gabriel Kojoian

Lawrence Radiation Laboratory
University of California
Berkeley, California

February 21, 1966

ABSTRACT

We report here the annihilation of antiprotons at rest in the Lawrence Radiation Laboratory's 15-inch deuterium-filled bubble chamber ($E_{\text{center of mass}} = 2.8137 \text{ Bev}$). The experiment was performed at the Bevatron. A total of 2071 events at rest were observed. The ratio of proton to neutron annihilations is 1.33 ± 0.07 . The reaction $\bar{p}d \rightarrow 3\pi^- + 2\pi^+ + n\pi^0 + p$ was examined extensively. The number of neutral pions was determined and it was found that the deviation between the statistical model and the experimental data was not overwhelming. The measured pion momentum and multiplicity distributions are in agreement with the Lorentz-invariant phase-space model when we consider an interaction volume of $\mathcal{V} = \lambda \mathcal{V}_0$ where $\mathcal{V}_0 = \frac{4}{3}\pi \left(\frac{\hbar}{m_{\pi}c}\right)^3$, $\lambda = 10$, and m_{π} is the mass of the pion. The momentum distribution of the observed recoil proton showed a marked difference from the internal momentum distribution of the deuteron. Secondary effects were considered because final state pion-proton interactions were not the major contributors to the annihilation dynamics. Stars yielding K mesons accounted for a fraction ($0.05 \pm .01$) of the total annihilation events observed.

I. INTRODUCTION

Dirac¹ introduced the concept of antiparticles by formulating a Lorentz-covariant equation for the electron, and his theory was confirmed in 1936 by discovery of the positron. Unsuccessful attempts were then made to discover antinucleons in cosmic radiation. In 1955 antiprotons were successfully produced at the Berkeley Bevatron by a team composed of Segre', Chamberlain, Wiegand and Ypsilantis.² Many experiments involving the annihilation of \bar{p} nucleus and $\bar{p}p$ ^{3,7,12,14} have been performed since then. Some of these interactions were antiproton annihilations at rest.^{4,6,13}

The experiment considered here involved sending a separated beam of \bar{p} 's, with initial momentum of 790 Mev/c, into the 15-inch deuterium-filled chamber. The antiproton loses energy by the usual processes of excitation and ionization as it passes through the liquid deuterium, and when the kinetic energy of the antiproton approaches zero it displaces the electron from the D_2 molecule and orbits the nucleus. The $\bar{p}d$ atom thus formed has a large angular momentum l and a principal quantum number $n \approx 25$. The antiproton then cascades down to lower (n, l) values through radiative transitions, external Auger processes and collisional de-excitations until it reaches an orbit which has a small radius compared to that of the atomic electron for deuterium. The size of this neutral atom ($\bar{p}d$) is such that it can penetrate the electron cloud of the neighboring atoms. Next, this neutral probe is exposed to a strong, non-central proton electric field. As a result, a Stark effect is induced, allowing the absorption process, for \bar{p} annihilations from

*why should it displace the electron?
Both e and \bar{p} could orbit the nucleus.*

rest, to take place essentially from the S state.

The annihilation is of particular interest because the reaction occurs in a pure $I = 1$ isospin state; therefore, a dependence on I-spin may be established by a study of the characteristics of this annihilation, and this dependence was the motivation for our study of antiproton-deuterium interaction at rest, some features of which are presented in the text.

II. EXPERIMENTAL PROCEDURE

A. Beam

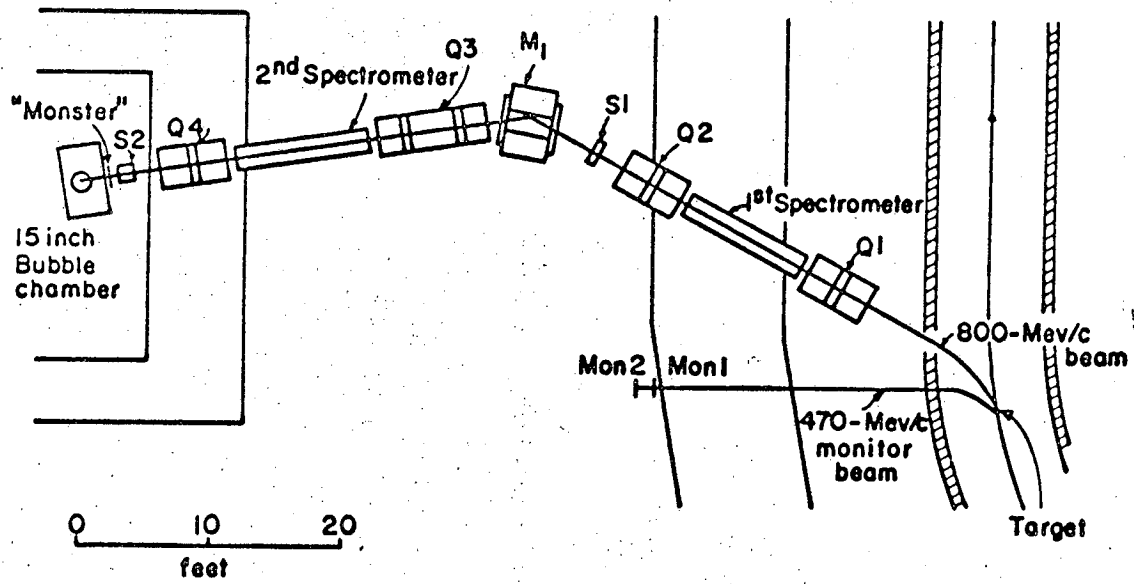
Only a brief summary of the 790 Mev/c antiproton beam (Fig. 1) will be given here because it has been described extensively elsewhere.⁸

The beam emerged from the Bevatron and was brought into parallel focus by Q1. After passing through the first parallel plate electrostatic separator it was brought into focus at S1 by Q2. At S1 the deflected pions were stopped by an 18-inch lead collimator, while the antiprotons passed through a 1/4" slit.

The bending magnet deflected the beam through an angle of 29 degrees, thus helping to eliminate much of the remaining background, since the undesirable particles which passed through the first slit were off the central momentum. The beam then passed through a second stage of separation, after which its momentum was reduced by a set of copper and graphite absorbers (located at the entrance of the bubble chamber), making it possible for the antiproton to interact at rest near the center of the chamber.

B. Scanning

A total of 2578 antiproton interactions, each consisting of four views, were observed and accepted as good events, according to the following criteria: only those events in the well-illuminated region of the bubble chamber and whose track curvatures could be adequately measured, were considered as good frames and thus acceptable for analysis. The average antiproton flux per picture was about 0.1 with a background of ~ 1 light track per



MU-26753

Fig. 1. Schematic diagram of the 790 Mev/c \bar{p} beam at the Bevatron.

picture. The dimensions of the fiducial volume were approximately 20 cm long and 23 cm wide as observed in view 1.

The antiprotons were easily distinguished from the background pions which either are minimum-ionizing or otherwise highly curved.

All of the film was scanned twice on a table specifically constructed for viewing film exposed to the 15-inch bubble chamber. Any two of four possible stereo views could be simultaneously projected onto this table and, by moving one of the projected views relative to the second, the approximate coordinate for any point of a track was determined. The following Table I indicates the efficiency for each scan as well as the overall efficiency.

C. Sketching and Measuring

First, a sketch was made of each antiproton annihilation, containing information specifying which set of the two stereo views out of the four available could be used for measuring. Next, the track coordinates in two of the four stereoscopic views were measured (by a servo auto-tracking device), digitized and punched onto IBM cards; the information was transferred to magnetic tapes which were used as the input to the data processing system.

D. Data Processing

1. Event Reconstruction

The events were analyzed by the IBM 7094 program PACKAGE, which consists of two parts: PANG⁹ and KICK.¹⁰ The PANG program reconstructs the polar angle ϕ , dip angle λ and momentum of each



TABLE I.

Scan Efficiency	0 Prong	1 Prong	2 Prong	3 Prong	4 Prong	5 Prong	6 Prong
1	77%	90%	95%	90%	93%	80%	93%
2	67	82	85	81	85	77	82
Overall	93	98	99	98	99	96	99

track from the measured points. A least squares fit of these points are made to a parabola in the x-y plane and to a straight line in the x-z plane. Momenta, dip and polar angles, with their attendant errors, were then calculated, the differences in the magnetic field along the track, Coulomb effects and optical corrections being included in these calculations. Measured quantities are not constrained by conservation equations; therefore, errors assigned to the track momenta are $\pm 15\%$ on the average.

2. Kinematical Fitting

The KICK program made a kinematical analysis of many-pronged events by imposing the constraints of energy and momentum balance on the tracks at the vertex assumed for the interaction. The KICK input data consisted of three dynamical variables for each track; these variables are assumed to be gaussian distributed. One dynamical variable is track curvature:

$$K_j = \frac{\pm 1}{|P_j| \cos \alpha_j} \quad \begin{array}{l} + \text{ incoming} \\ - \text{ outgoing} \end{array} \quad (1)$$

the next is dip angle (λ); and another is azimuthal angle (ϕ).

A least squares fit of the event was made. The output data consists of an adjusted value for each dynamical variable and a chi-square value for the selected hypothesis. The χ^2 is defined as follows:

$$\chi^2 = \sum_{j=1}^n \left(\frac{x_j - x_j^m}{\sigma_j} \right)^2, \quad (2)$$

n = number of tracks

x_j^m = measured dynamical variable

x_j = adjusted dynamical variable

σ_j = standard deviation associated with each variable

The χ^2 is at a stationary point for all variations within the interval Δx_j about x_j , consistent with the kinematic constraints. The value for χ^2 is the measure of the probability that the selected hypothesis is valid, and this value was used to help resolve the ambiguity in determining the number (0, 1, 2 or more) of neutral pions accompanying the charged products of annihilation.

III. ANALYSIS OF DATA

A. Identification of Events at Rest

The great majority of events observed were annihilations of \bar{p} 's, at rest, in deuterium.

Figure 2 is a scatter plot of the inverse of the initial momentum versus track length for over 300 incident antiprotons that annihilated upon interaction with deuterons. The unbroken curve shows the locus of points for interaction momenta of zero Mev/c. A cluster of events in the neighborhood of this curve can be clearly seen: less than 5% of the 2071 events designated as at rest were in flight. The total number of $\bar{p}d$ annihilations observed, excluding strange particle production, was 2578.

B. Analysis of Events

890 of those events at rest had an odd number of charged pions (i.e., total pion charge $Q = -1$). Thus, this class of events with an odd total of pion charges can be regarded as an unambiguous example of antiproton - neutron annihilation. Included in these 890 events were groupings which had one, three and five charged pions in the final state. Within each of these groupings the number of recoil protons either stopping in the chamber, leaving the chamber or simply not observable because of insufficient momentum, is as follows:

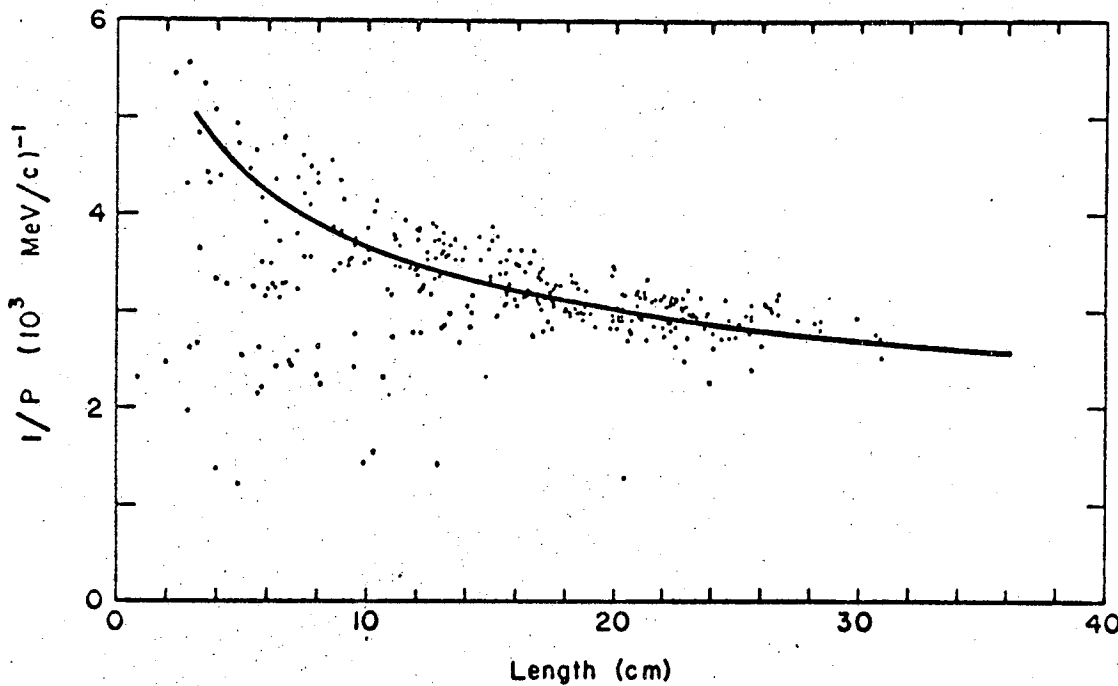


Fig. 2. Scatter plot of inverse of measured initial momentum versus observed length of each antiproton track which terminated in an annihilation event. The solid curve shows the expected behavior, deduced from the range-energy relation, for annihilations occurring at rest. MUB-7721

11

Events with One Charged Pion

50 protons Stopped in chamber
42 protons Left chamber
66 protons Not observable (insufficient momentum)

Events with Three Charged Pions

152 protons Stopped in chamber
85 protons Left chamber
288 protons Not observable (insufficient momentum)

Events with Five Charged Pions

61 protons Stopped in chamber
32 protons Left chamber
114 protons Not observable (insufficient momentum)

Among the above-listed three groupings 263 events had recoil protons which stopped in chamber; 468 events did not have an observable recoil proton because the momentum for each proton was less than 80 Mev/c; and 159 proton recoils did not stop in the chamber and were identified on the basis of bubble density. This latter sample is subject to error from π^+ mesons with large dip angles and K^+ tracks misidentified as protons. However, the distribution of proton polar angles (Fig. 3) and dip angles (Fig. 4) are consistent with isotropy, and pion contamination is thus negligible.

The estimate of K^+ tracks misidentified as protons is arrived at by analyzing the $(\bar{p}p)$ annihilations at rest. The final

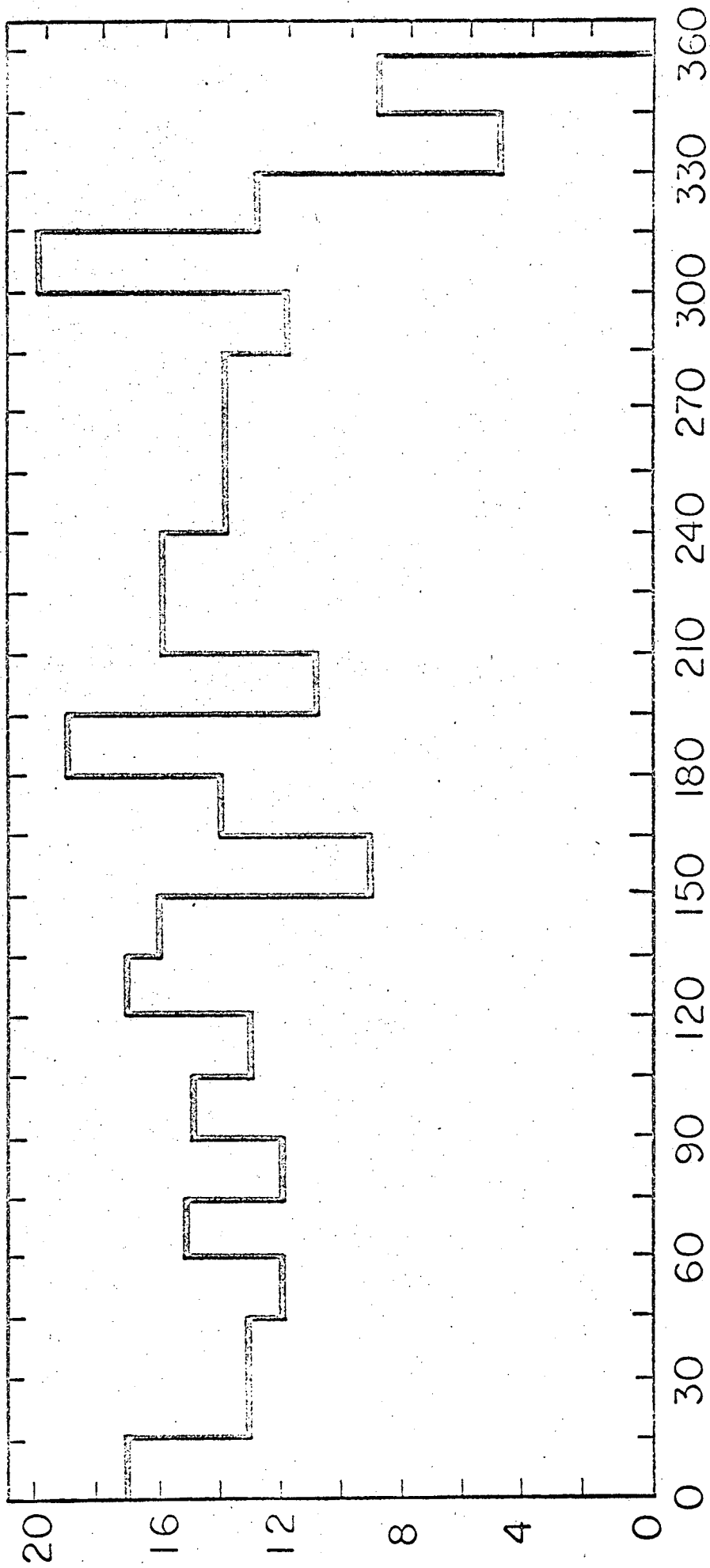


Fig. 3. Distribution of polar angles of outgoing proton from $p\bar{d}$ annihilations yielding three and five charged pions.

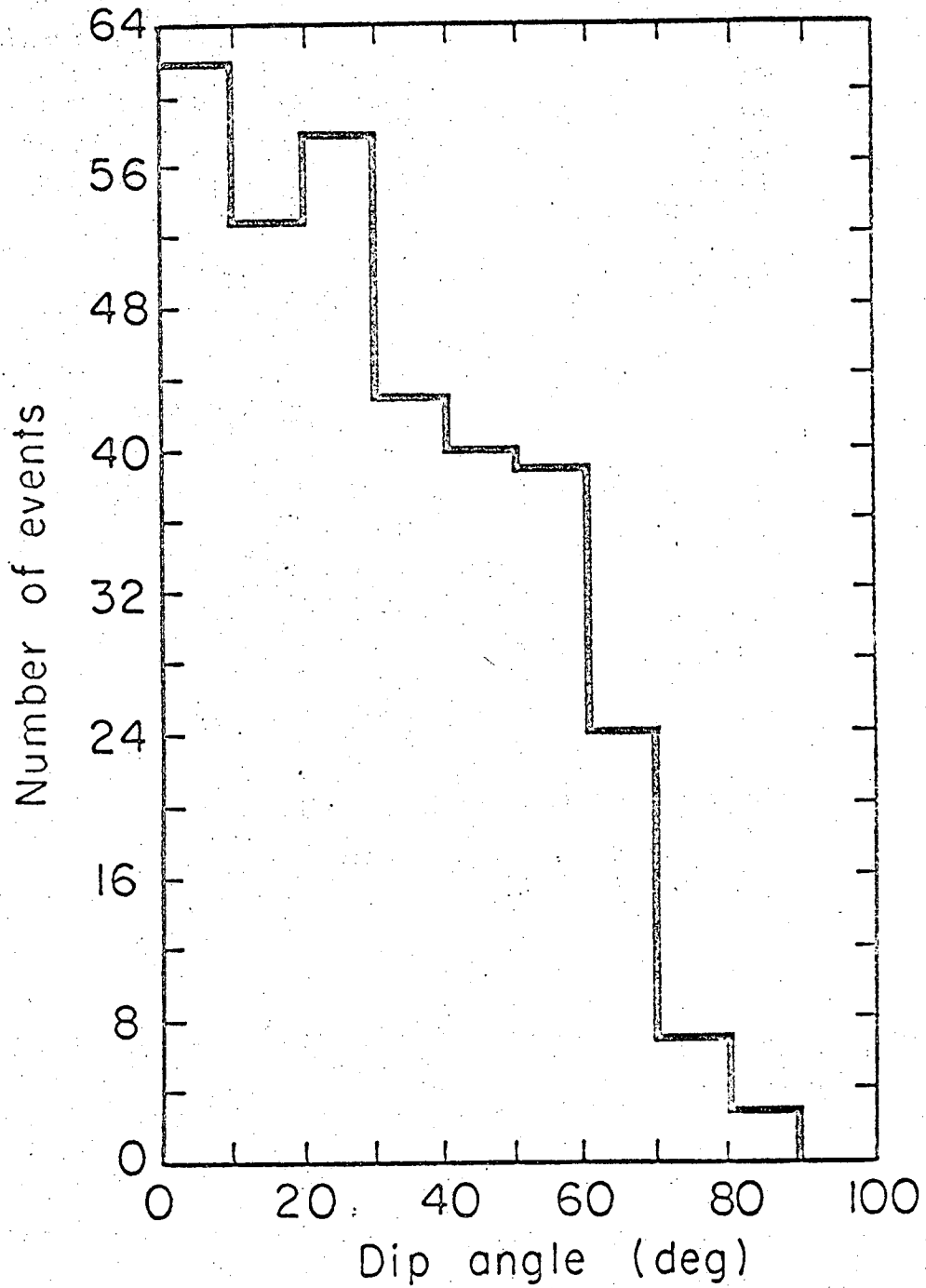
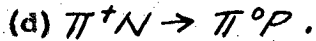
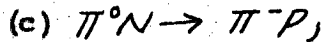
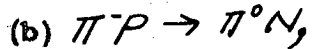
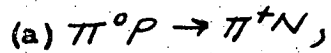


Fig. 4. Distribution of dip angle of outgoing proton from $\bar{p}d$ annihilations yielding three and five charged pions.

state of this interaction may include K^+ mesons, but no protons. 1235 ($\bar{p}p$) interactions were recorded: of this number, 1181 had pions and no strange particles; 6 resulted in Λ^0 production; and the remaining events had K mesons in the final state. According to Armenteros et al.⁶ 6.8% of the ($\bar{p}p$) annihilations at rest result in K meson production. Assuming that $\sim 1/2$ of the strange particles are positive K mesons, then approximately 40 K^+ 's are to be expected. The misidentification of these heavy mesons as protons is most likely in the momentum interval extending between 300-500 Mev/c. According to the phase-space distribution of momenta approximately 40% of the total, or about 16 K^+ 's, lie within this momentum interval. However, 9 K^+ 's from ($\bar{p}p$) annihilations were observed as having momenta within this range; therefore, 7 ± 3 K^+ 's are estimated to be included among the particles identified as protons. Thus, the misidentified positive K mesons are not expected to produce significant distortions in the observed momentum distribution of the proton.

Of the total sample of annihilations at rest 1181 were examples of proton annihilation, including all those events with an even number of charged pions in the final state, as well as 62 events with 0-prongs. The ratio of proton to that of neutron annihilations is 1.33 ± 0.07 . This ratio is not sensitive to pion-nucleon final state effects. The following charge exchange reactions are possible as a result of $\bar{p}d$ interactions:



For cases (a) and (b) a $\bar{p}n$ annihilation simulates a proton absorption; whereas in cases (c) and (d) a $\bar{p}p$ annihilation simulates a neutron absorption. According to the principle of detail balance the reaction rates for (a) - (d) and (b) - (c) are expected to be approximately equal. Assuming that charge independence is correct and that isotopic spin is a conserved quantity the square of the matrix elements for the reaction (a) - (c) and (b) - (d) are the same. Therefore, reaction rates indicated in these four cases are approximately equal. Assuming a statistical distribution of charges,¹¹ and relating it to the five pion mode:

$(\bar{p}p)$ annihilations result in $1.61 \pi^+$, $1.61 \pi^-$
and $1.76 \pi^0$;

the $(\bar{p}n)$ case produces $1.2 \pi^+$, $2.2 \pi^-$ and $1.6 \pi^0$,
on the average.

In effect, these values indicate a near-zero neutron-proton exchange.

C. Analysis of Five-Prong Annihilations

To test the hypothesis that $(\bar{p}n)$ interactions at rest may proceed via an intermediate vector meson,¹⁵ 67 events (from a total of 127 observed), with 5 charged pions and a recoil proton, were analyzed to determine the number of neutral pions produced. Of

the 127 events, 67 satisfied the fiducial criteria, and the remaining did not. Other examples of neutron annihilation were not included because it was not possible to unambiguously decide the number of neutral pions.

This interaction was identified as a $(\bar{p}n)$ by the usual method of determining the consistency of measured quantities with the kinematics of the reaction.

Of the 67 acceptable events:

13 were unambiguously identified as having no π^0 's; that is, they satisfied the following criteria: a χ^2 acceptable for 4 constraint fits and measured missing energy and mass within one standard deviation of zero (see Figs. 5, 6b, and 6a);

23 events were unambiguously identified as having 1 π^0 ; that is, they each had a χ^2 acceptable for a one constraint fit and a missing mass within one standard deviation of 135 Mev (see Figs. 7 & 6a);

6 events were unambiguously identified as having 2 or more π^0 's where measured quantities satisfied the following criteria: the missing mass was greater than 270 Mev and more than 4 standard deviations from 135 Mev. In fact, the smallest value of missing mass is 356 Mev. The lowest exhibited by these events, when tested for the 1 π^0 hypothesis, was 6.48;

25 events were ambiguous: of this number, 5 exhibited chi-squares which allowed for both the zero π^0 and 1 π^0 hypothesis, and 2 of these 5 had missing masses consistent with 1 standard deviation from zero (and were placed in the zero π^0 bin), and the remaining 3 had missing masses consistent with 1 standard deviation from the π^0 mass (and were placed in the 1 π^0 bin);

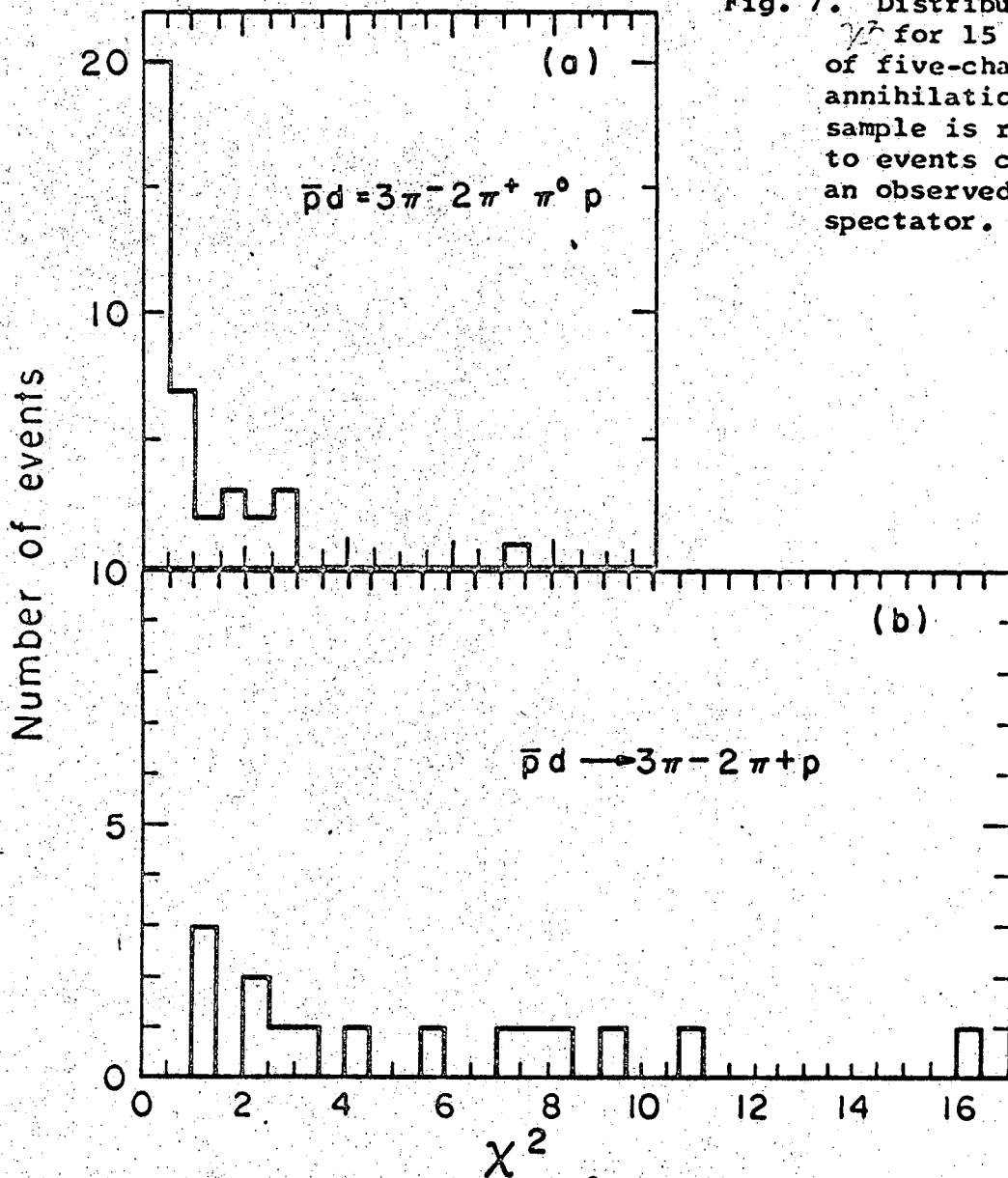
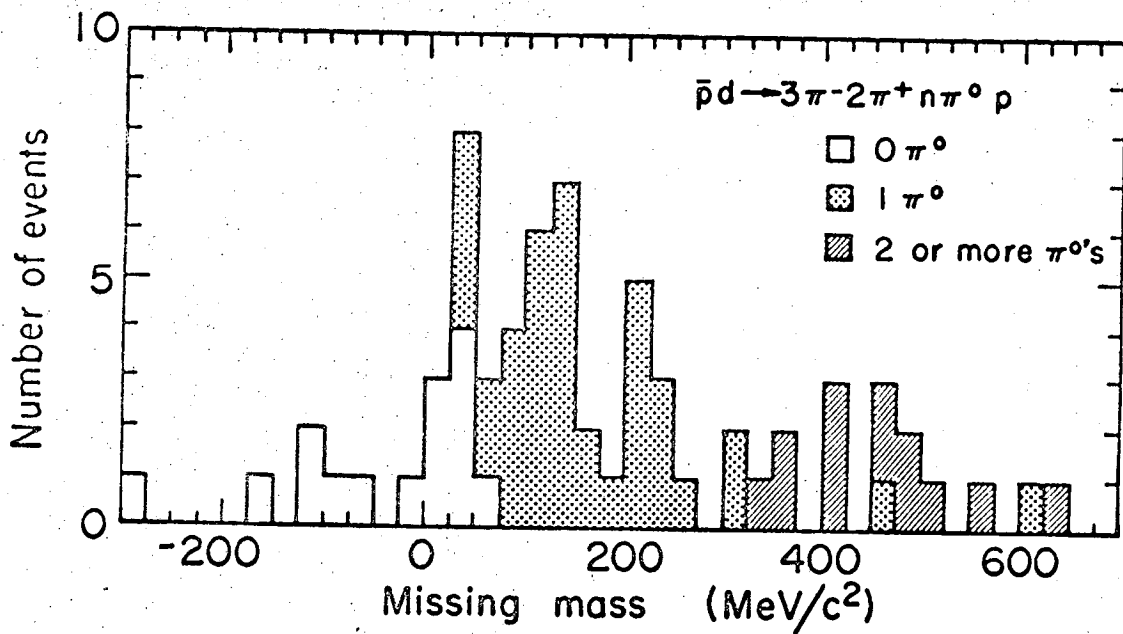


Fig. 5. Distribution in χ^2 for 15 events of five-charged pion annihilations. The sample is restricted to events containing an observed proton spectator. MUB-7720

Fig. 7. Distribution in χ^2 for 15 examples of five-charged pion annihilations. The sample is restricted to events containing an observed proton spectator.



MUB-7719

Fig. 6a. Distribution of missing mass $(\sqrt{(\text{missing energy})^2 - (\text{missing momentum})^2})$ in 67 examples of $\bar{p}d$ annihilations yielding five charged pions and a proton spectator. Identification of the number of missing π^0 's is shown by the appropriate shading in the histogram.

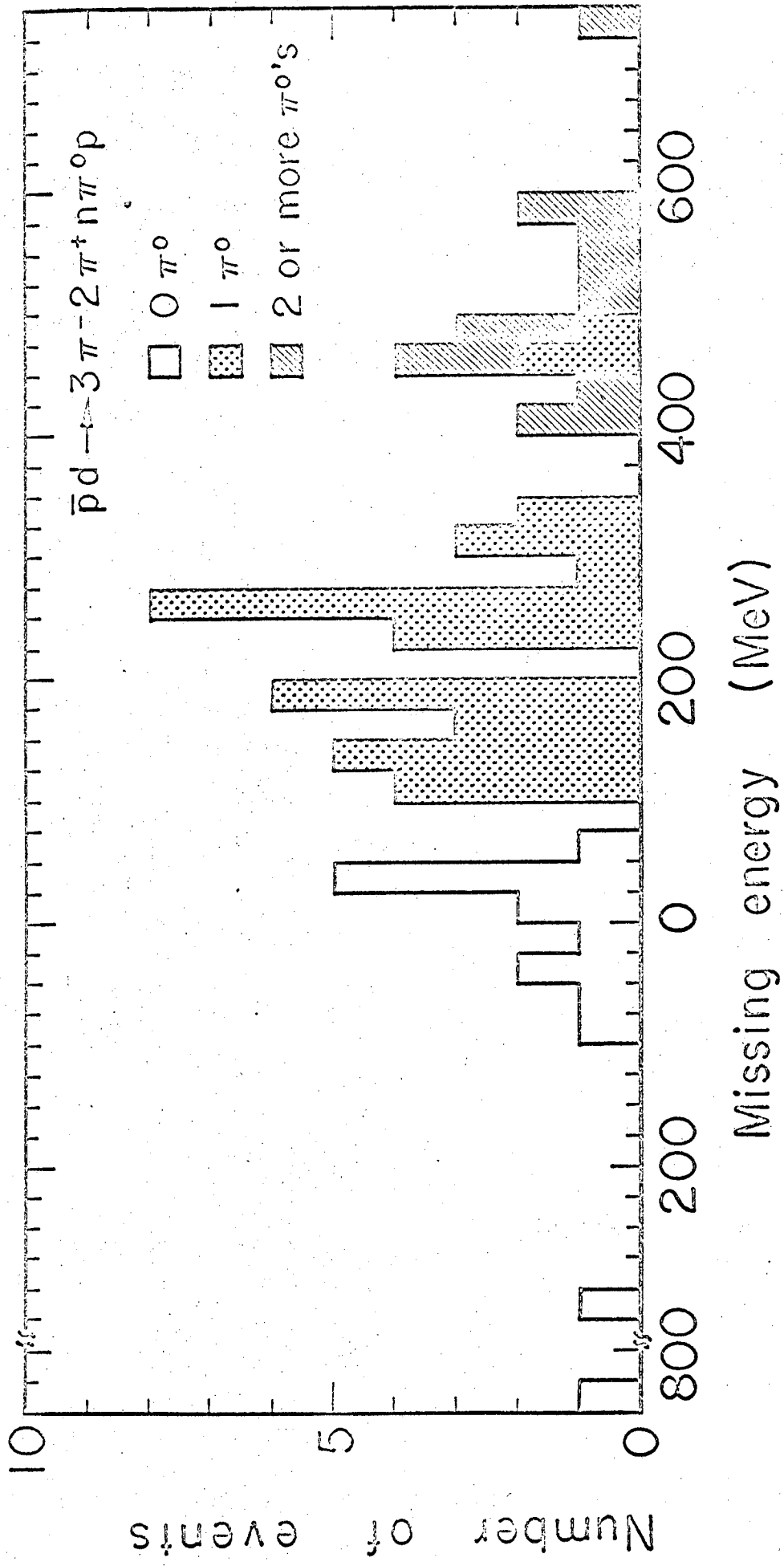


Fig. 6b. Distribution of missing energy in 67 examples of $\bar{p}d$ annihilations yielding five charged pions and a proton spectator. Identification of the number of missing π^0 's is shown by the appropriate shading in the histogram.

The remaining 20 events were ambiguous in that they contained 1, 2 or more π^0 's (they were placed in bins according to their missing mass squared values). Missing mass squared histograms were made from all 42 unambiguous events. A natural grouping that separates the two or more π^0 events from all others is indicated in Fig. 8. This separation occurs near 350 Mev. Consequently, we conclude that 13 events have a single neutral pion, and the remaining 7 have 2 or more.

The final results are:

<u>No. of Neutral Pions</u>	<u>No. of Events</u>
0 π^0 's	15
1 π^0	39
2 or more π^0 's	13

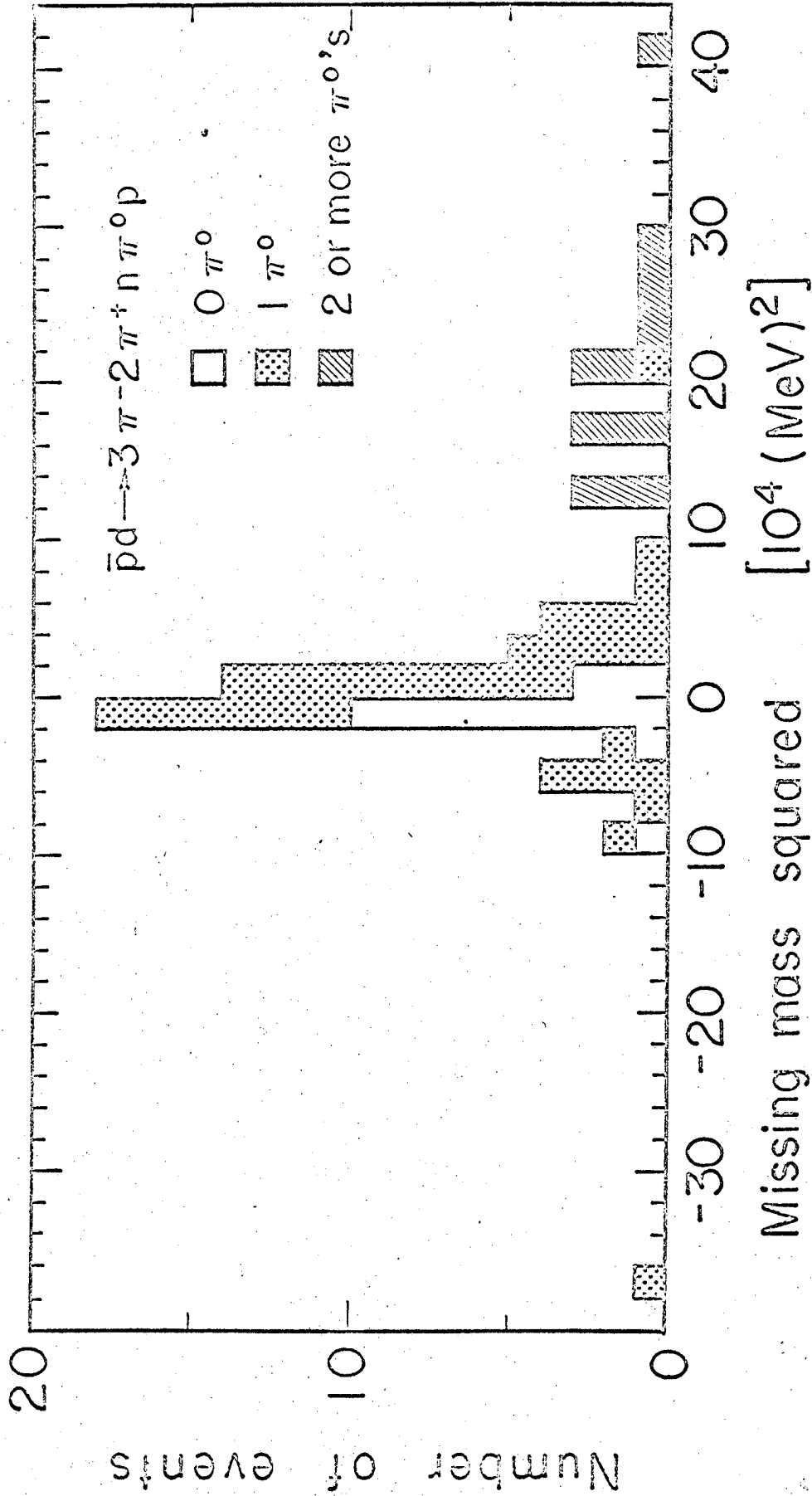


Fig. 8. Distribution of missing mass squared in 42 examples of $\bar{p}d$ annihilations yielding five charged pions and a proton spectator. Identification of the number of missing π^0 's is shown by the appropriate shading in the histogram.

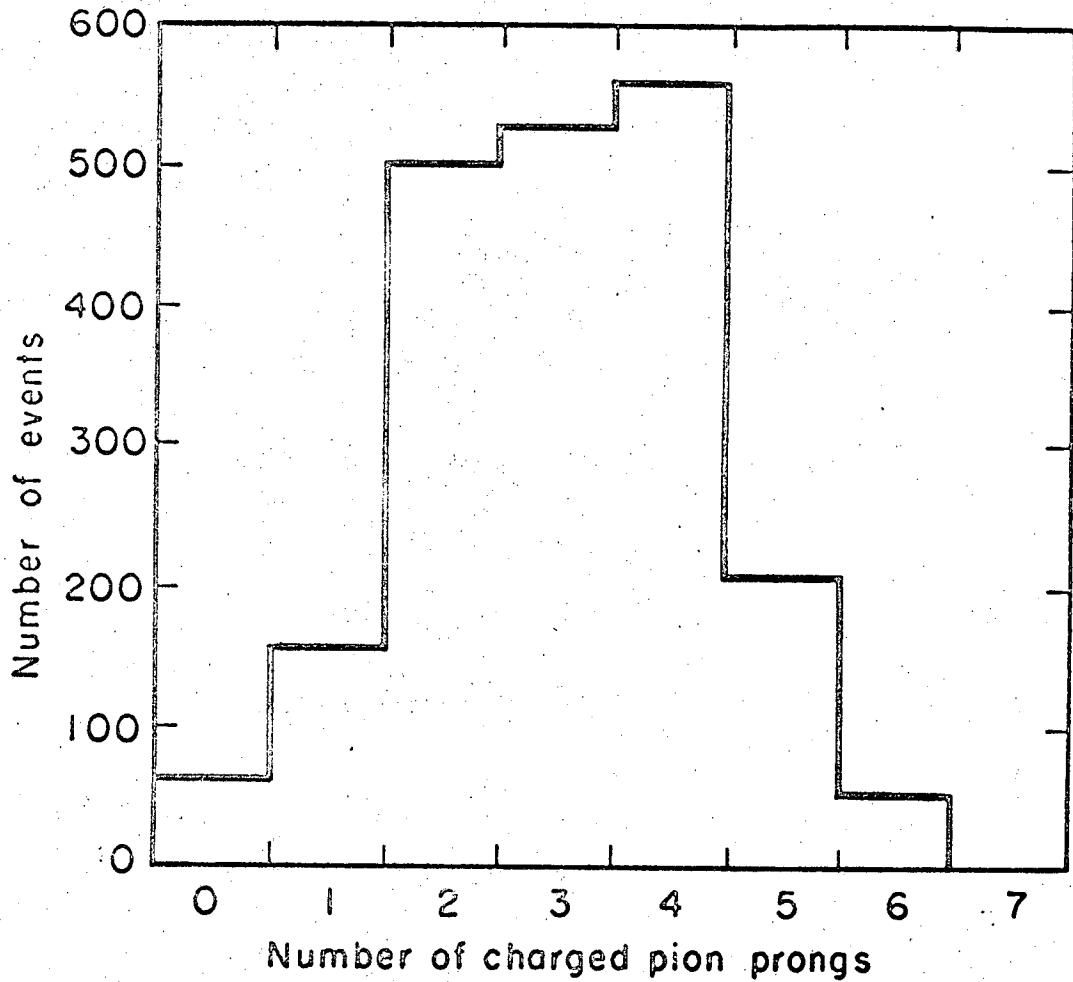
IV. DISCUSSION OF RESULTS

A. Pion Multiplicity Distribution

Pion multiplicity distribution of 2071 events is shown in Fig. 9. The average pion multiplicity in the annihilation process, according to the Fermi model using covariant phase-space integrals, for an interaction radius of 2.2 fermi's, is 5.11. The mean number of observed charged particles is $\overline{m}_{\pi^\pm} = 3.07 \pm 0.08$. Assuming that the energy distribution for neutral pions is the same as that for charged pions, then the average total multiplicity is $\overline{m}_{\pi^0} = 5.11 \pm .30$. This value is consistent with the calculated value of 5.11 and with the results of Horwitz et al.⁷ The mean number of observed charged prongs in proton annihilation is 3.03 ± 0.10 ; in neutron annihilation it is 3.11 ± 0.12 .

In the simple statistical model the total nucleon-antinucleon rest energy of $2M_{\text{n}}c^2$ is released into an interaction volume Ω . Then, statistical equilibrium among different modes is established and pions of corresponding final states are released according to the statistical distribution, which is proportional to the probability that all the particles are simultaneously available within the interaction volume $\Omega = \lambda \Omega_0$, where $\Omega_0 = 4/3 \pi \left(\frac{h}{m_\pi c} \right)^3$, and λ is the only adjustable parameter. The value $\lambda \approx 10$ is chosen in order to fit the observed average number of pions produced in the annihilation process.^{16,17} However, this value $\lambda \approx 10$ overestimates the relative probability of K meson production. Why?

is it because $m_K > m_\pi$?



MUB-7714

Fig. 9. Multiplicity distribution of the charged-pion prongs in 2071 antiproton-deuteron annihilations at rest. Events with identified K mesons are not included.



The statistical distribution for n-pions in an isotopic spin state I is:¹⁶

$$S_m(I) = A \frac{G_n(I)}{n!} \left[\frac{2m_\pi \Omega}{(2\pi)^3} \right]^m F_m(W) \quad (3)$$

Here:

$\hbar = c = 1$, and A is a constant independent of the n;

$G_n(I)$ = total number of isotopic spin states available for a given n;

$n!$ = for n identical particles, $n!$ states are equivalent under interchange in each I-spin state;

$\left[\frac{2m_\pi \Omega}{(2\pi)^3} \right]^m$ = relates to the probability of finding

the n-pions in a plane wave momentum eigenstate in Ω , the interaction volume.

$$F_m(W) = \int \int \prod_{j=1}^m \frac{d^3 p_j}{\omega_{\pi_j}} \delta^3 \left[\sum_{j=1}^m \vec{p}_j \right] \delta \left[W - \sum_{j=1}^m \omega_{\pi_j} \right] \quad (4)$$

is the covariant phase-space integral. W = total energy in the center of mass system, \vec{p}_j and ω_{π_j} are the momentum and energy of the i^{th} particle. This integral is calculated by the iteration technique⁵ (see Appendix 1).

In the Fermi model the only quantities rigorously conserved are the total linear momentum and energy of the system; the conservation of angular momentum, parity and other observables which may influence the results of the annihilation process are not included.

B. Pion Momentum Distribution

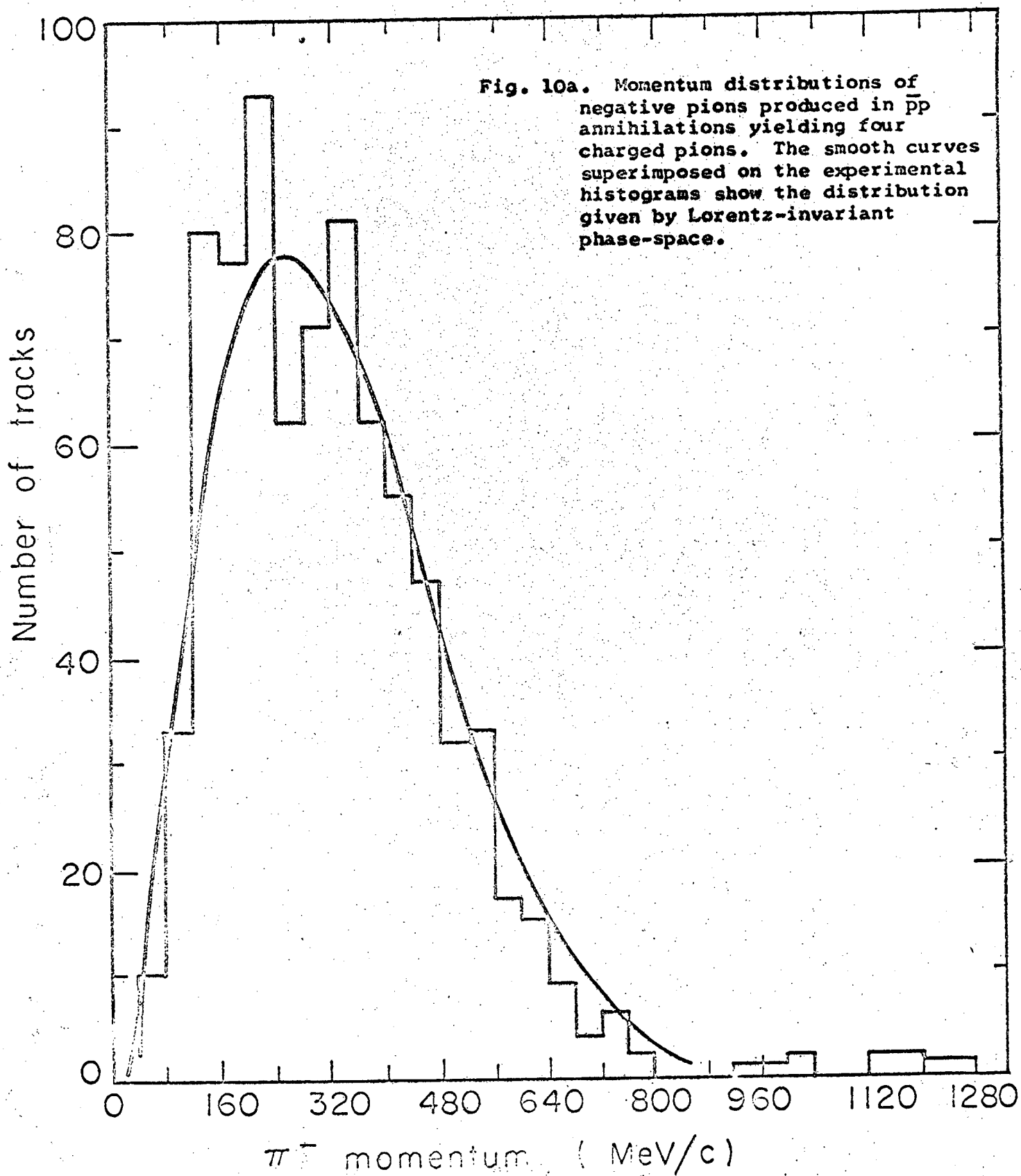
Momentum distribution of charged pions from proton annihilations are shown in Figs. 10a, 10b, 11a, and 11b. There is no essential difference between the results presented here and those of Ref. 6, in which antiprotons annihilated with free protons.

Momentum distributions resulting from neutron annihilations are shown in Figs. 12a, 12b, 13a, and 13b. A corresponding phase-space distribution accompanies each graph. There is no significant deviation between the experimental and statistical distributions.

The pion momenta are from measured track curvatures and not from fitted data. A small fraction of the total number of pions had momenta greater than that allowed by kinematics, which we attribute to poor measurement accuracy. However, when the error in the measurement is taken into consideration the magnitudes of the momenta are within the allowable kinematical limits.

C. Pion-Pion Correlations

Effective mass distributions ($\pi^+ \pi^-$) were made with pions from final states which had 3 and 5 charged pi-mesons (Figs. 14a and 14b). Included in these graphs are the appropriate phase-space



11-465-1

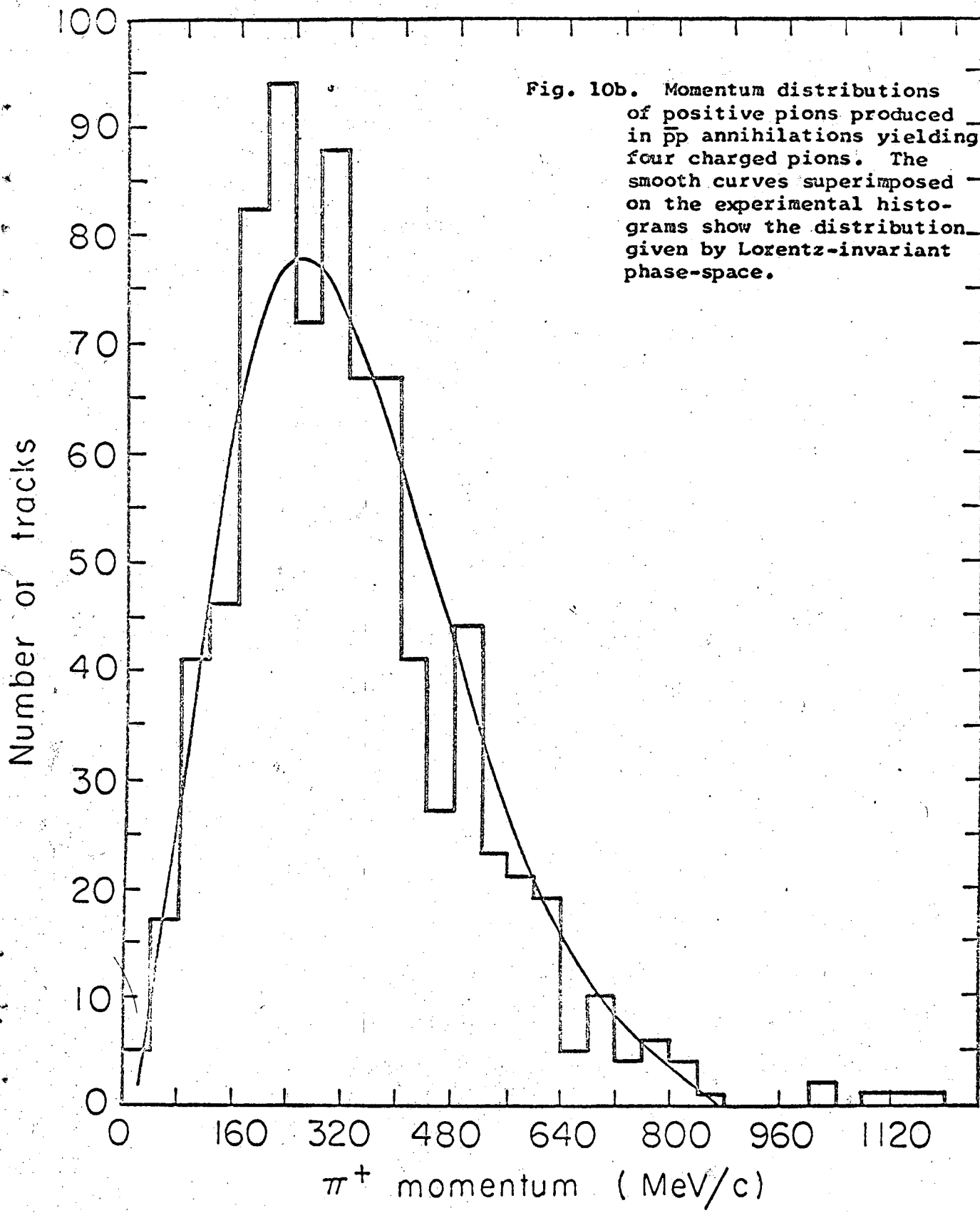


Fig. 10b. Momentum distributions of positive pions produced in $\bar{p}p$ annihilations yielding four charged pions. The smooth curves superimposed on the experimental histograms show the distribution given by Lorentz-invariant phase-space.

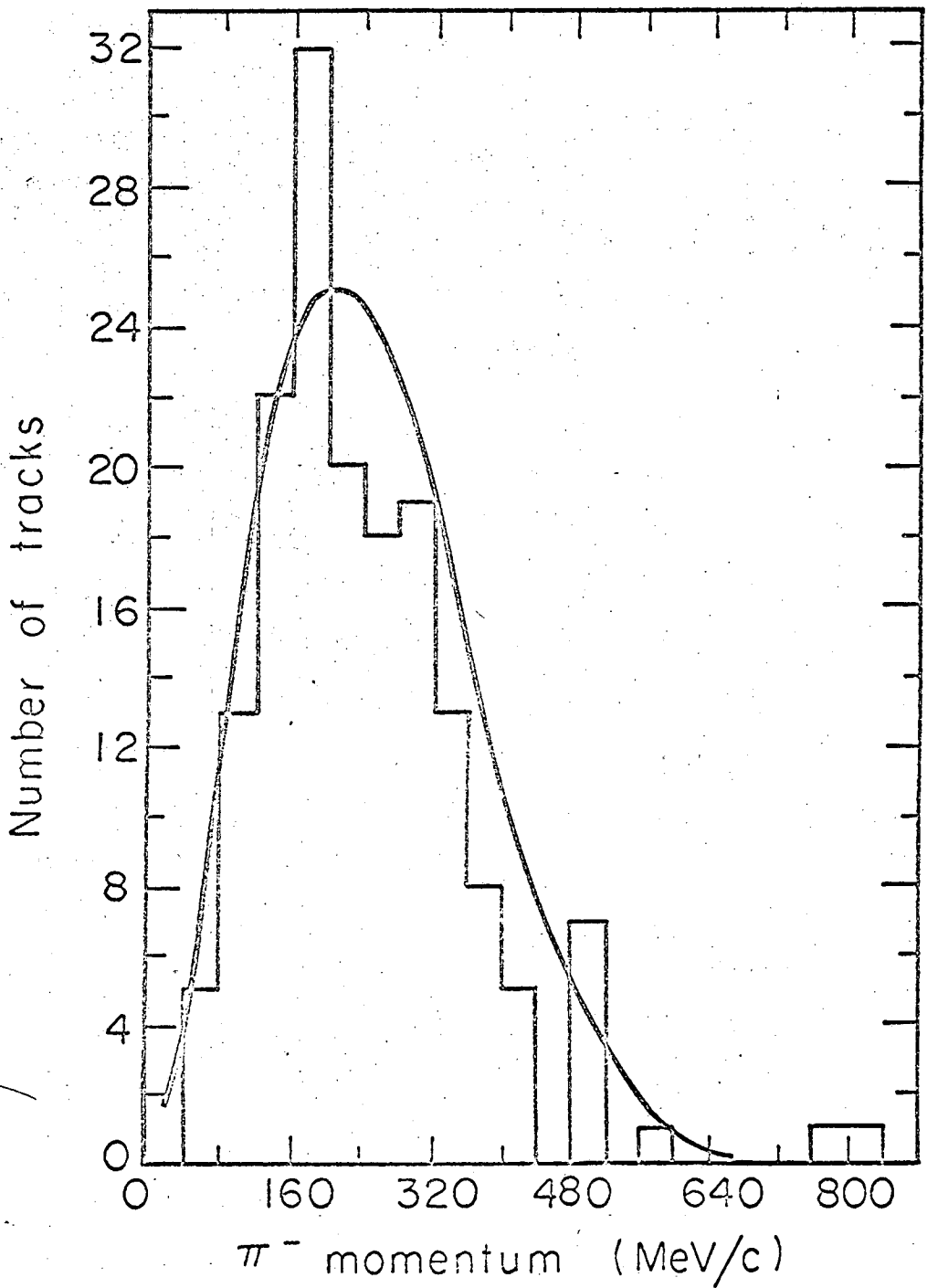


Fig. 11a. Momentum distributions of negative pions produced in $\bar{p}p$ annihilations yielding six charged pions. The smooth curves superimposed on the experimental histograms show the distributions given by Lorentz-invariant phase-space.

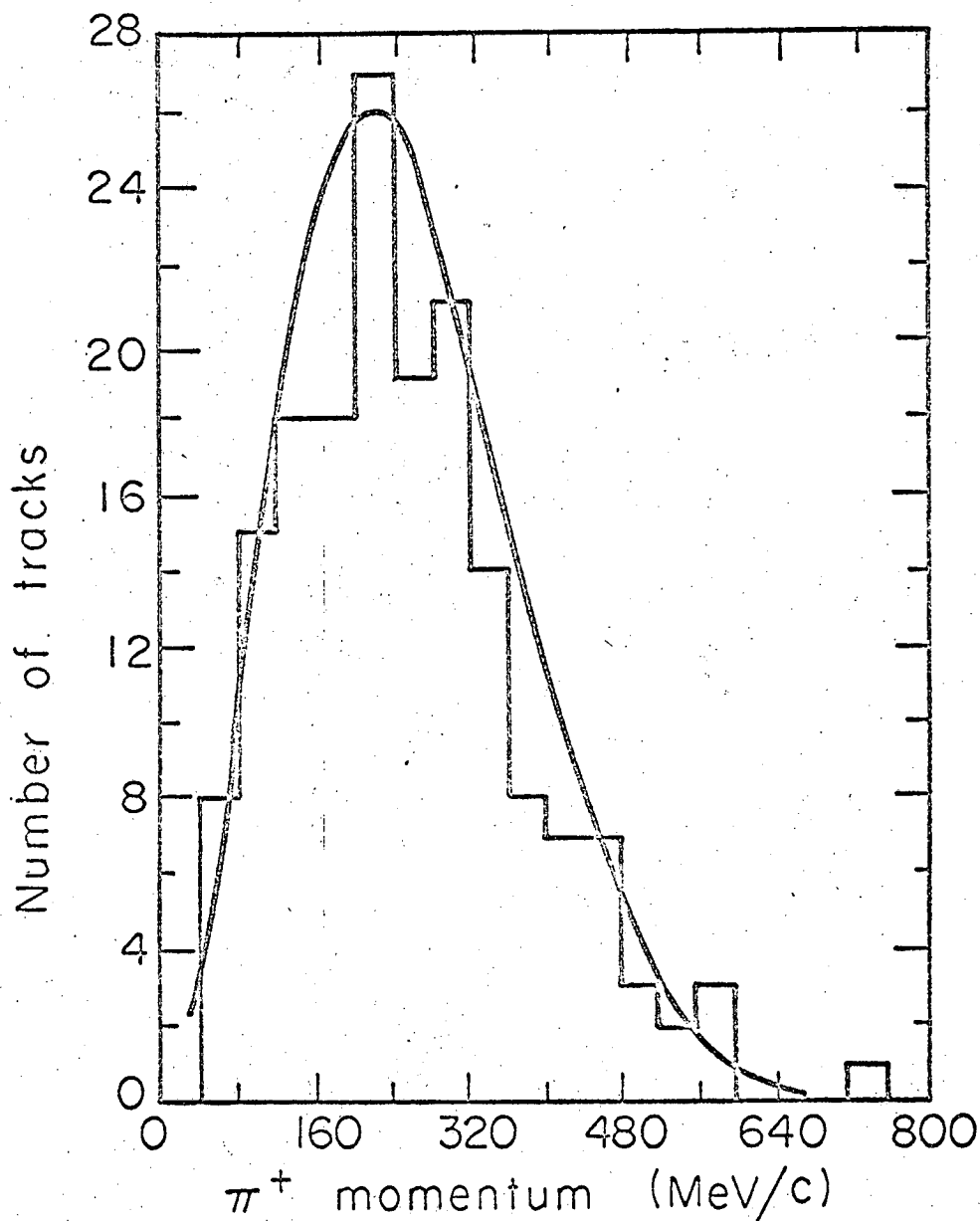


Fig. 11b. Momentum distributions of positive pions produced in $\bar{p}p$ annihilations yielding six charged pions. The smooth curves superimposed on the experimental histograms show the distribution given by Lorentz-invariant phase-space.

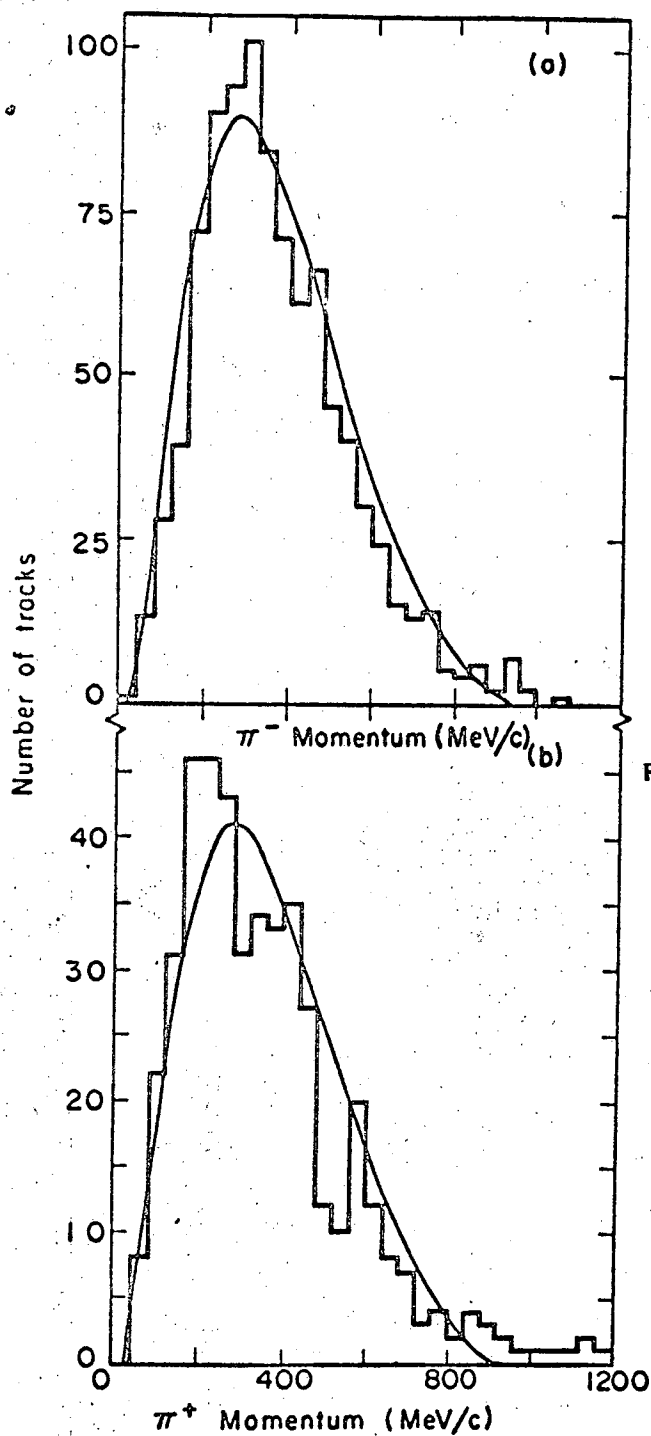


Fig. 12a. Momentum distributions of negative pions produced in antiproton-neutron annihilations yielding three charged pions. The smooth curves superimposed on the experimental histograms show the distribution given by Lorentz-invariant phase-space.

Fig. 12b. Momentum distributions of positive pions produced in antiproton-neutron annihilations yielding three charged pions. The smooth curves superimposed on the experimental histograms show the distribution given by Lorentz-invariant phase-space.

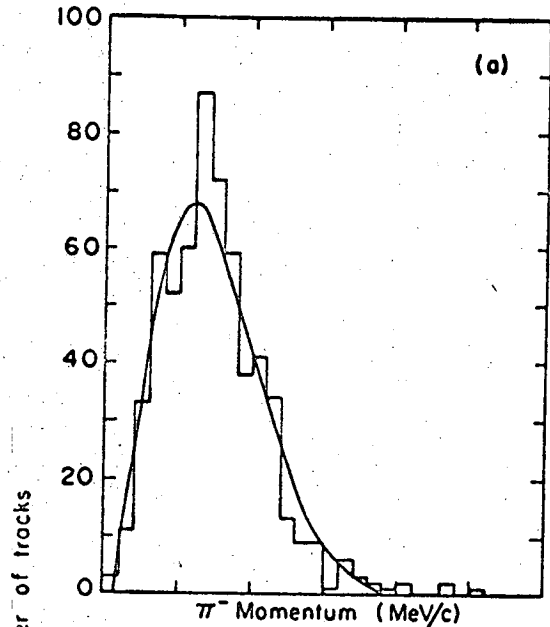


Fig. 13a. Momentum distributions of negative pions produced in $\bar{p}n$ annihilations yielding five charged pions. The distributions given by Lorentz-invariant phase-space are superimposed upon the experimental histograms.

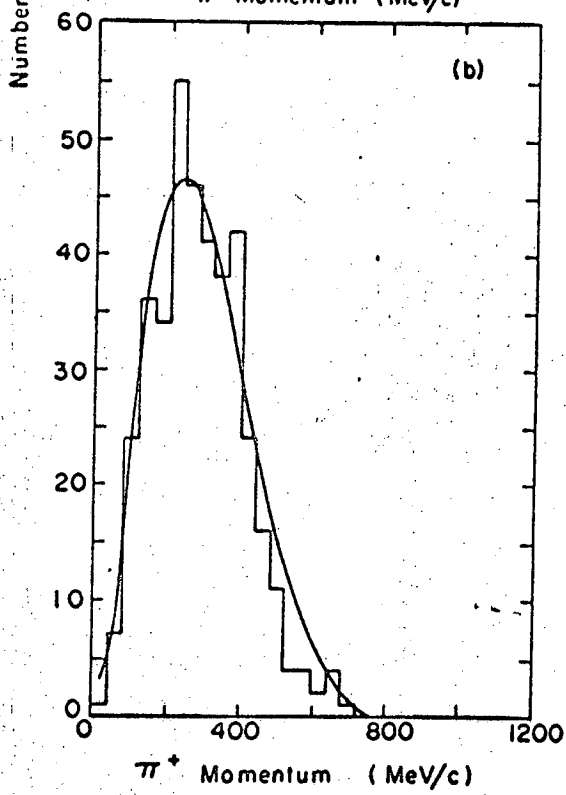


Fig. 13b. Momentum distributions of positive pions produced in $\bar{p}n$ annihilations yielding five charged pions. The distributions given by Lorentz-invariant phase-space are superimposed upon the experimental histograms.

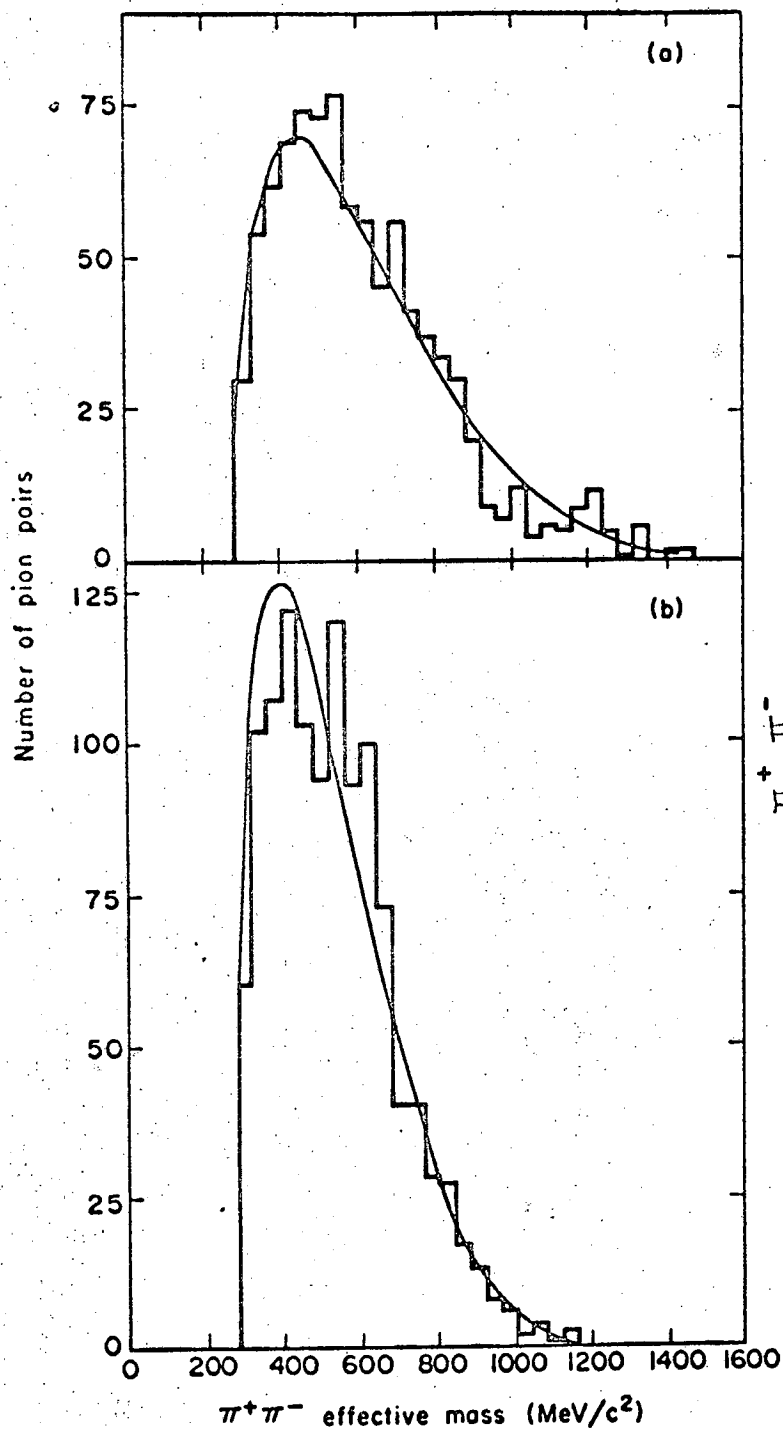


Fig. 14. Effective mass of $\pi^+\pi^-$ pairs produced in $\bar{p}n$ annihilations yielding (a) three charged pions and (b) five charged pions. All possible $\pi^+\pi^-\pi^+\pi^-$ combinations were used for each event. The smooth curves show the distribution obtained from the statistical model.

plots. Measured, not fitted, quantities were used. The results indicate only a small amount of resonant state production and no significant deviation between statistical and experimental distributions.

D. Multi-Pion Events

The antiproton-proton state consists of an equal mixture of isotopic-spin states $I = 0$ and $I = 1$, and antiproton-neutron is in a pure $I = 1$ state; this indicates that the annihilation ratio is responsive to the isotopic-spin dependence of the annihilation matrix elements. Using the simple statistical assumption that the annihilation rate $R(\bar{p}p)$ for $\bar{p}p$ is the statistical sum of $I = 0$ and $I = 1$, and assuming no interference between these channels, then:

$$R(\bar{p}p) = \frac{1}{2} R(I = 0) + \frac{1}{2} R(I = 1), \tag{5}$$

whereas the antiproton-neutron annihilation rate $R(\bar{p}n) = R(I = 1)$. The relative rates for the annihilation into n-pions is as follows:

$$\rho_n = \frac{R_n(\bar{p}p)}{R_n(\bar{p}n)} = \frac{\frac{1}{2} N_n(I=0) |M_n(I=0)|^2 + \frac{1}{2} N_n(I=1) |M_n(I=1)|^2}{N_n(I=1) |M_n(I=1)|^2} \tag{6}$$

M_n 's are matrix elements for transitions into the respective isospin states. The weight factors $N_n(I = 0)$ and $N_n(I = 1)$ are the number of linearly independent n-pion states in $I = 0$ and $I = 1$. These numbers are listed in Table II.¹⁸ These states are not distinguished by their momenta or configurations, but in fact are independent of

all quantum numbers, except for isotopic spin. Unsuccessful attempts have been made to calculate these weight factors in an extended Fermi model,¹⁹ which distinguishes itself from the classical one by including the conservation of angular momentum and parity.

Now let us construct a model whose matrix elements are not functions of I-spin. In this model:

$$\rho_m = \frac{R(\bar{p}p)}{R(\bar{p}N)} = \frac{1}{2} \left\{ \frac{N_m(I=0)}{N_m(I=1)} + 1 \right\} \quad (7)$$

The average value of $\rho_m = 0.71$. This value is relatively independent of the number of pions (see Table II) and is not consistent with the experimental result ($\rho_{exp} = 1.33$). Using the experimental result for ρ in Eq. (7) gives the following value for the ratio:

$$\frac{R(I=0)}{R(I=1)} = 1.66, \quad (8)$$

which indicates that on the average, the $I = 0$ state is more prevalent than $I = 1$.

Chadwick et al.¹³ have concluded from their study of the annihilation reaction $\bar{p} + p \rightarrow \rho^0 + \pi^0$ that, for this interaction, $I = 0$ is the dominant state.

TABLE II. Ratio for annihilations into n pions.

<u>n</u>	<u>$N(I = 0)$</u>	<u>$N(I = 1)$</u>	<u>P_n</u>
2	1	1	1.0
3	1	3	0.67
4	3	6	0.75
5	6	15	0.70
6	15	36	0.71

E. Five-Prong Annihilations and Selection Rules

The results of the CERN experiment,⁶ a study of the final-state $K^0\bar{K}^0$ from $(\bar{p}p)$ interaction at rest, indicate a predominance of S-state capture. If the nucleon-antinucleon annihilations proceed via a vector meson intermediary the 3S_1 -state would dominate.¹⁵ Berman and Oakes¹⁵ have examined this hypothesis, the consequences of which are particularly simple for $(\bar{p}n)$ annihilations at rest. $(\bar{p}n)$ is in a pure $I = 1$ state and the only known vector meson with $I = 1$ is the rho meson. It follows then that this interaction can result only in an even number of pions. This hypothesis was tested for 67 events having five charged pions and a recoil proton (see Section III-C). The results are:

<u>No. of Neutral Pions</u>	<u>No. of Events</u>	<u>Corresponding Statistical Prediction</u>
0 π^0 's	15	26 forbidden by Berman & Oakes
1 π^0	39	33 allowed by Berman & Oakes
2 or more π^0 's	13	8 (forbidden for even numbers of π^0 's, by Berman & Oakes)

Our experimental results are not in complete agreement with the radius dependent ($r = 2.2f$) statistical model;¹⁶ however, the deviations are not overwhelming. The model which indicates that the nucleon-antinucleon annihilation proceeds via a vector meson intermediary may not be valid at all interaction energies. It is clear that the rho meson exchange is not the only dynamical mechanism in antiproton-neutron annihilation at rest. \bar{p} annihilations

are "at rest" with respect to the center of mass of the deuteron and not necessarily with the individual nucleons. In general these nucleons are in motion with the incident particle, and some P-state annihilation can be expected. This effect obscures the relevance of the Berman and Oakes model.

F. Proton Momentum Distribution

1. Two-Body Antiproton Interactions

Plotted in Figs. 15 and 16 is the momentum spectrum of recoil protons from the reaction $\bar{p}d \rightarrow n\pi + p$. This distribution includes a total of 732 protons resulting from annihilations into 3 and 5 charged pions, 402 of which had momenta ≤ 80 Mev/c; that is, they were insufficient to produce a detectable track in the bubble chamber. Events with a single charged pion were excluded in order to minimize errors in identification of the positive track. Because of the possible inclusion of pions misidentified as protons this class of events would favor the high momentum region. In this group, about 27% of the recoil protons left the chamber, as opposed to about 15% for the 3 and 5 charged pion final states (see Section III-B).

The spectator model assumes that the incident antiproton interacts with one of the two nucleons in the deuteron, and that the presence of the second nucleon does not contribute to the annihilation dynamics. In such a situation the particles in the deuteron are likely to be some "large" distance apart during the interval of interaction, and the low-lying momentum states would be the most

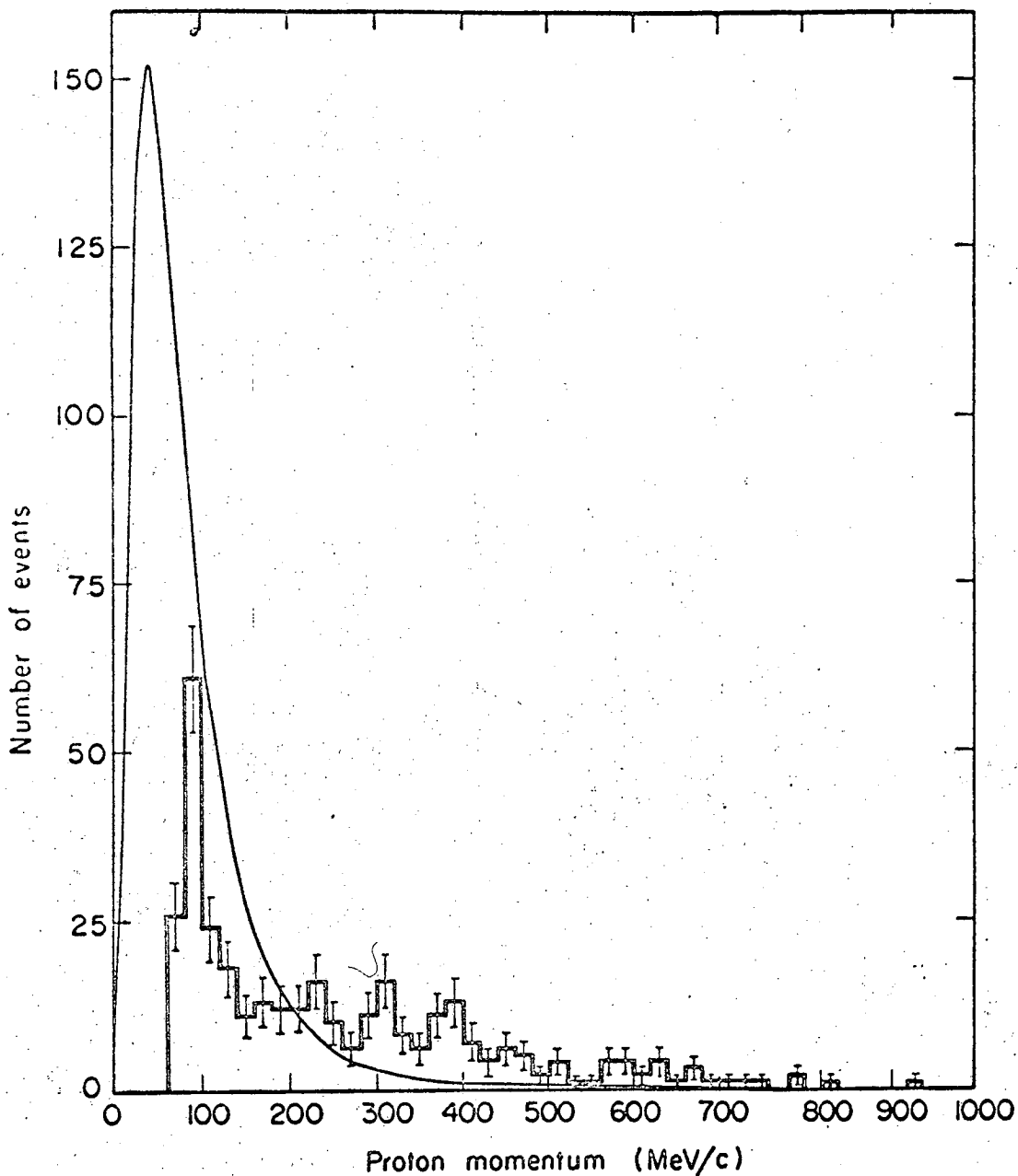


Fig. 15. Momentum distribution of observed, identified proton-spectator tracks resulting from $\bar{p}d$ annihilations into three and five charged pions. The smooth curve is the nucleon internal-momentum distribution obtained from a "Hulthén" deuteron wavefunction. MUB-7718

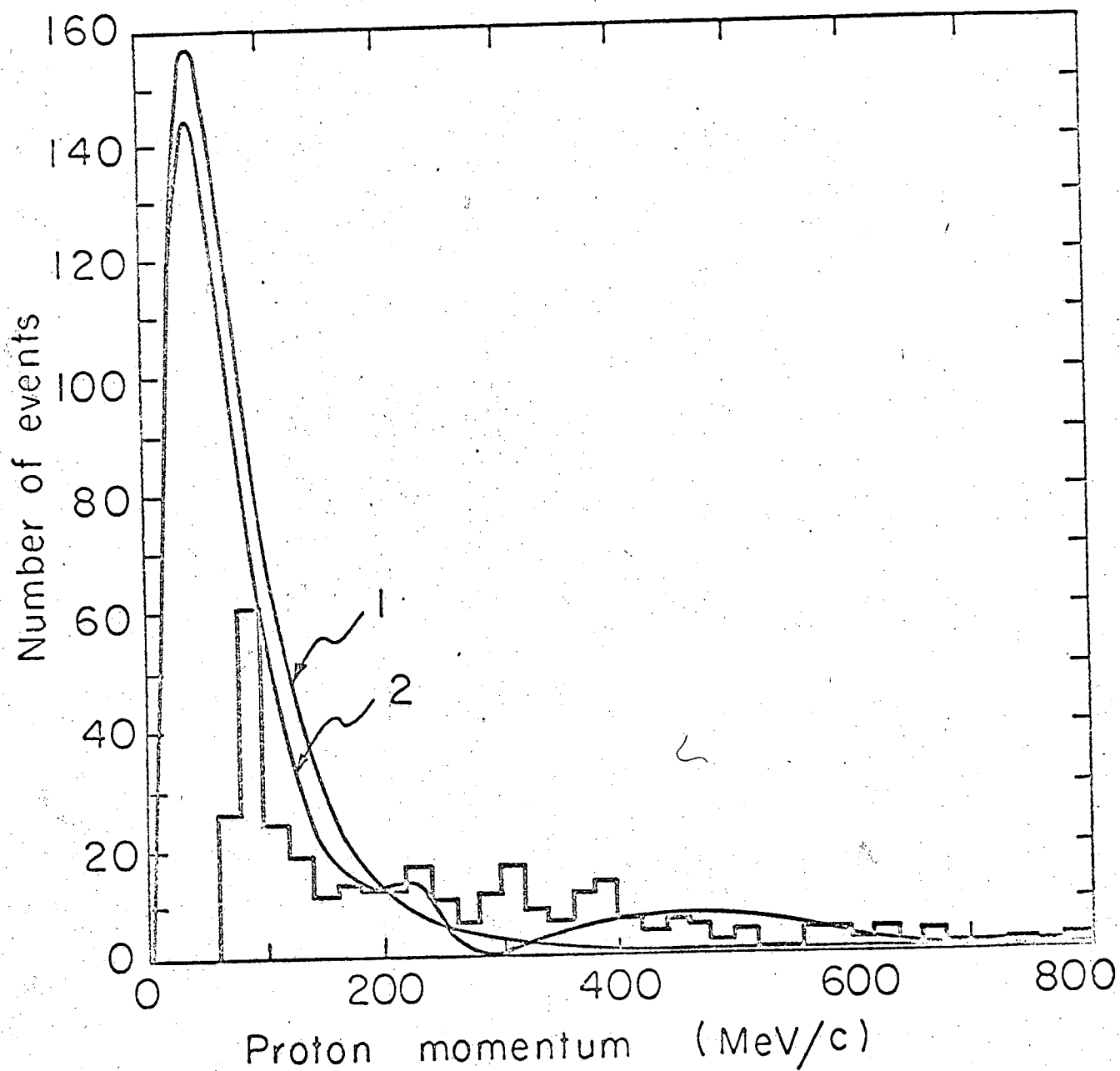


Fig. 16. Momentum distribution of observed, identified proton-spectator tracks resulting from $\bar{p}d$ annihilations into three and five charged pions. The smooth curves are the nucleon internal-momentum distributions obtained from (1) a "Hulthen" deuteron wave function and (2) a "Hulthen" simulated hard core wave function.

likely ones. The Hulthén wave function²⁰ may be expected to give the observed distribution. It has the following form in coordinate space:²¹

$$\psi_H(r) = \left[\frac{2\alpha\beta(\alpha+\beta)}{\beta-\alpha} \right]^{1/2} \frac{e^{-\alpha r} - e^{-\beta r}}{r}, \quad (9)$$

and the representation of this function in momentum space is:²¹

$$\psi_H(k) = \frac{2}{\beta-\alpha} \left[\frac{\alpha\beta(\alpha+\beta)}{\pi} \right]^{1/2} \left[\frac{1}{\alpha^2+k^2} - \frac{1}{\beta^2+k^2} \right], \quad (10)$$

where

$$\alpha^2 = \frac{2m_r(-E)}{\hbar^2} = \left(\frac{1}{4.31} f^{-1} \right)^2, \quad (11)$$

$E = -2.226$ Mev, the binding energy of the deuteron and m_r is the reduced mass of the deuteron. $\beta = 1.31f^{-1}$ is the Hulthén parameter and $K =$ proton momentum. The unbroken curve of Fig. 15 is a plot of $|\psi_H(k)|^2 k^2$.

Figure 15 is a comparison between the observed momentum distribution and that plot given by the phenomenological ground state deuteron wave function of Hulthén. The internal momentum distribution of the proton deviates significantly from the observed spectrum. The experimental data shown in Fig. 15 indicates an excess of high

momentum recoil protons. Of 732 such protons 165 had momenta greater than 200 Mev/c, while the predicted number, using the Hulthén wave function, is 40. It is evident that the agreement between the Hulthén wave function and the observed shape is poor.

Essentially, all protons whose recoil momenta was ≤ 250 Mev/c were stopped in the chamber; all others were identified on the basis of bubble density. The disparity between the observed and the phenomenological ground state wave function cannot be accounted for by misidentification of tracks in the final state (see Section III-B).

The momentum distribution given by Eriksson, Hulthén and Johansons' wave form²² differs only slightly from the corresponding Hulthén function, and thus is not shown. The essential difference between the phenomenological functions^{21,22} is that the effects of the D wave are incorporated in the Eriksson, Hulthén and Johansons wave form.

An attempt to simulate the effect of a hard core is made by incorporating into the Hulthén wave form a smoothly varying function $f(r)$, which has the following properties:

$$\begin{aligned}
 f(r) &= 0 & 0 < r < r_c \\
 f(r) &= \sin \frac{\pi}{\lambda} \left(\frac{r - r_c}{d - r_c} \right) & r_c < r < d \\
 f(r) &= 1 & d < r < \infty
 \end{aligned} \tag{12}$$

where it was assumed that $r_c = 0.4f$, the hard core radius, and d is the distance at which the Hulthén wave function is not altered by a hard core. The coordinate representation of the wave function

is now:

$$\psi(r) = \frac{N}{\sqrt{4\pi}} \left\{ \frac{e^{-\alpha r} - e^{-\beta r}}{r} \right\} f(r), \quad (13)$$

where N is the normalization factor.

The form of this function in momentum space is:

$$\Phi(k) = \frac{N}{\sqrt{2\pi^2}} \left\{ \psi_\alpha(k) - \psi_\beta(k) \right\}, \quad (14)$$

where

$$\psi_\alpha(k) = \left[e^{-\alpha d} (\cos kd + \frac{\alpha}{k} \sin kd) \times \left\{ \frac{1}{\alpha^2 + k^2} + \frac{\alpha^2 + k^2 + \frac{\pi^2}{4(d-r_c)^2}}{(\alpha^2 - k^2 + \frac{\pi^2}{4(d-r_c)^2})^2 + 4\alpha^2 k^2} \right\} - \frac{\pi}{2(d-r_c)} e^{-\alpha r_c} \frac{(2\alpha \cos kr_c + (\alpha^2 - k^2 + \frac{\pi^2}{4(d-r_c)^2}) \sin kr_c)}{(\alpha^2 - k^2 + \frac{\pi^2}{4(d-r_c)^2})^2 + 4\alpha^2 k^2} \right], \quad (15)$$

and for $\psi_B(k)$, we replace α by β . The proton momentum distribution is:

$$\rho(k) = 4\pi k^2 |\phi(k)|^2 \quad (16)$$

(see Appendix B).

A value of 1.15f for d was chosen in order to give a good fit to the data. This value for d indicates that the wave functions, with and without the simulated hard core, have the same shape, beginning at about 3 hard core radii. If the magnitude of d is less than 1.15f, the resultant effect is greater because it approaches a region in which the wave function has a larger value. Above 1.15f the resultant effect is small because now it approaches a region in which the wave function has a smaller value.

Superimposed on the observed data in Fig. 16 is the form $|\psi_H(k)|^2 k^2$ and $\rho(k)$, the proton momentum distribution of a Hulthén simulated hard core. As expected, the function $\rho(k)$ fits as well as the Hulthén in the low-lying momentum region and it has a reasonable behavior in the high momentum region. But it clearly does not describe the state of the system in the neighborhood of 300 Mev/c, which includes 16% of the events.

An incident particle with momentum of order of 100 Mev/c with respect to the center of mass of the target nuclei will have a λ between 3 and 4 fermi's. This is approximately equal to the most likely distance separating the nucleons in the deuteron. Apparently

the spectator model with the Hulthén wave function is not valid for interactions when the relative momentum between target and incident particle is much less than 100 Mev/c; it is more likely that the incident particle will interact with both nucleons simultaneously. The Hulthén simulated hard core with the spectator model works better than expected; however, the reason for this behavior is not known.

The two-body annihilation model (the third nucleon a spectator to the annihilation interaction) does not completely describe the antiproton-deuteron annihilation; therefore, some secondary effects must be considered in an attempt to understand the observed momentum distribution.

Three modes which could contribute to the distortion between the observed momentum distribution and that plot given by the phenomenological ground state deuteron wave function of Hulthén (Fig. 15) are:

(a) Final state interactions -- isobar production,

$$\bar{p}d \rightarrow (n-1)\pi_0^+ + N_{3,3}^* \quad ;$$

↘ π^+p

(b) Three-body antiproton interactions,

$$\bar{p}d \rightarrow (\bar{p}Np) \rightarrow n\pi_0^+ + p \quad ;$$

(c) Bound state,

$$\bar{p}d \rightarrow (\bar{p}N)_{bound} + p \rightarrow n\pi_0^+ + p \quad .$$

2. Final State Interactions

The effect on the momentum spectrum of the proton (a result of resonant π^+p interactions, from $\bar{p}d$ annihilations into three and five charged pions in the final state) was studied. We will now develop a form of the proton momentum distribution, indicating how it was modified by final-state phase-space and enhancement factors. The cross section for production of n-pions and a proton with momenta \underline{dp}_i and \underline{dQ} , respectively, is:

$$d\sigma = N \int \prod_{i=1}^m \frac{dp_i}{\omega_i} \frac{dQ}{E_Q} \delta\left[\sum_{i=1}^m p_i + Q\right] \delta\left[\sum_{i=1}^m \omega_i + E_Q - M_{\bar{p}} - M_d\right] |T_{fi}|^2 \quad (17)$$

where $T_{fi} = (\Psi_f, t \Psi_i)$, the transition matrix between initial and final states. The notations being used throughout are as follows:

\underline{dp}_i = momentum interval for i^{th} pion

ω_i = total energy for i^{th} pion

\underline{dQ} = momentum interval for proton

E_Q = total energy for proton

$M_{\bar{p}}$ = mass of antiproton

M_d = mass of deuteron

N = normalization factor

$\Psi_i \sim \Psi(r_1, R) \Psi_d(r)$, where $r = r_3 - r_2$

\underline{E} = momentum of deuteron center of mass

\underline{r}_1 = antiproton spatial coordinate

\underline{r}_2 = neutron spatial coordinate

r_3 = proton spatial coordinate

z_i = pion spatial coordinate

$$\psi_f \sim \frac{e^{iQ \cdot r_3}}{(2\pi)^{3/2}} \phi(z_i) \quad (18)$$

$$(\psi_f)^\dagger \psi_i \sim \int_{\text{all space}} \frac{e^{-iQ \cdot r_3}}{(2\pi)^{3/2}} \phi(z_i)^\dagger \psi(r_1, R) \psi_d(r_2) dV \quad (19)$$

where

$$dV = \prod_{i=1}^n d^3 z_i d^3 r_3 d^3 r_1 d^3 R \quad (20)$$

Now assume that the proton is a spectator to the annihilation process in deuterium, and then its r_3 integral may be done immediately:

$$\begin{aligned} & \int_{\text{all space}} d^3 r_3 e^{-\frac{iQ \cdot r_3}{\hbar}} \psi_d(r_3 - r_1) = \\ & \int_{\text{all space}} d^3 r e^{-\frac{iQ \cdot r_2}{\hbar}} \frac{e^{-iQ \cdot r}}{(2\pi)^{3/2}} \psi_d(r_2) = \\ & e^{-\frac{iQ \cdot r_2}{\hbar}} \int_{\text{all space}} \frac{e^{-iQ \cdot r}}{(2\pi)^{3/2}} \psi_d(r_2) d^3 r = \\ & e^{-\frac{iQ \cdot r_2}{\hbar}} \psi_d(Q) \end{aligned} \quad (21)$$

where $\Psi_d(Q)$ = Fourier transform of $\Psi_d(r)$. Recalling that \bar{p} and \bar{d} interacted at rest, the \bar{p} momentum and the deuteron momentum $\bar{E} = 0$, so that:

$$T_{fi} = \Psi_d(Q) \delta\left[\sum_{i=1}^m p_i + Q\right] t_{fi} \quad (22)$$

Now the cross section has the following form:

$$d\sigma = N \int \prod_{i=1}^m \frac{d^3 p_i}{\omega_i} \frac{d^3 Q}{E_Q} \delta\left[\sum_{i=1}^m p_i + Q\right] \delta\left[\sum_{i=1}^m \omega_i + E_Q - M_p - M_d\right] |t_{fi}|^2 |\Psi_d(Q)|^2 \quad (23)$$

The momentum spectrum $P(Q) = \frac{d\sigma}{dQ}$, where

$$P(Q) = \frac{|\Psi_d(Q)|^2 Q^2}{E_Q} \int \prod_{i=1}^m \frac{d^3 p_i}{\omega_i} \delta\left[\sum_{i=1}^m p_i + Q\right] \delta\left[\sum_{i=1}^m \omega_i + E_Q - M_p - M_d\right] |t_{fi}|^2 \quad (24)$$

If we consider a statistical model, $|t_{fi}|^2 = \text{constant}$, then the momentum spectrum of the recoil proton is modified in the final state by phase-space factors. These factors insure four-momentum conservation and are purely a kinematical effect.

Next, consider the $\bar{p}d$ annihilation as entering into a resonant region in the final state. We assume the same enhancement factor for each and every pion, without regard to charge, in the production mode under study, thereby overestimating the effect of the resonance on the proton spectrum. In such a formulation the $\pi^0 p$, $\pi^- p$ and $\pi^+ p$ pairs contribute similarly to the enhancement factor, whereas the $N_{\frac{3}{2}, \frac{3}{2}}^*$ state is a resonant state of the appropriate $\pi^+ p$ pairs only.

Now the matrix element $|t_{fi}|^2 = \prod_{i=1}^n G(\omega_i)$, where $G(\omega_i)$ is the weighting factor for the i^{th} meson (due to the resonant final state interaction). According to Gillespie:²³

$$G(\omega_i) = (\text{CONSTANT}) \exp\left\{2(\omega_i - u_i) \frac{P}{\pi} \int_{u_i}^{\infty} \frac{\delta(\omega') d\omega'}{(\omega' - u_i)(\omega' - \omega_i)}\right\} \quad (25)$$

where P indicates the principal value of the integral; $\delta(\omega')$ is the phase shift for $\pi^+ p$ scattering in the $I = 3/2$ and $J = 3/2$ state at a pion energy ω' ; ω_i is the total energy of the i^{th} pion, and u_i is the pion mass.

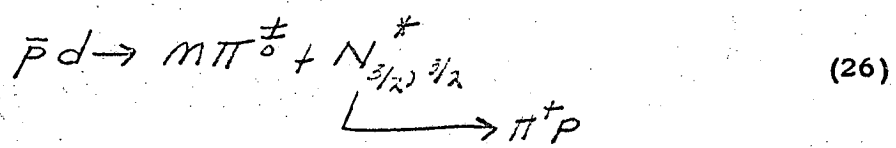
A Monte Carlo technique was utilized to generate events in which the momenta of all the particles involved were distributed according to phase-space. The rate of annihilations into a specific final state was weighted both by the appropriate product of weighting factors and by the square of the phenomenological deuteron wave function in momentum space;²² this tends to increase the yield for a $\pi^+ p$ system near the resonant region. Figure 17

shows the momentum distribution of protons generated from these Monte Carlo calculations, from the Hulthén distribution and from our observed results.

There is no significant difference between the phenomenological deuteron internal momentum distribution and the results of the final-state interaction calculations; in fact, no displacement towards the high momentum region is evident in the distribution characterized by the Monte Carlo calculations; and, rather, enhancement is indicated near 140 Mev/c.

Figure /7 shows an inadequate number of recoil protons in the neighborhood of 160 Mev/c, and it is difficult to conclude that final-state interactions produce this effect. Below 150 Mev/c the shape of the recoil proton spectrum is affected by measurement biases and observational difficulties, especially at large dip angles. It is apparent from Fig. /7 that final-state pion-proton interactions do not produce an excess of high momentum protons.

Another technique for studying the effect of pion-proton interactions in the final state is to start with the assumption that a fraction of the annihilation proceeds in the following manner:



The formation of isobars resulting from three-body annihilations can be expected to yield high momentum protons. The spectrum for the protons produced from N* decay was calculated, using the

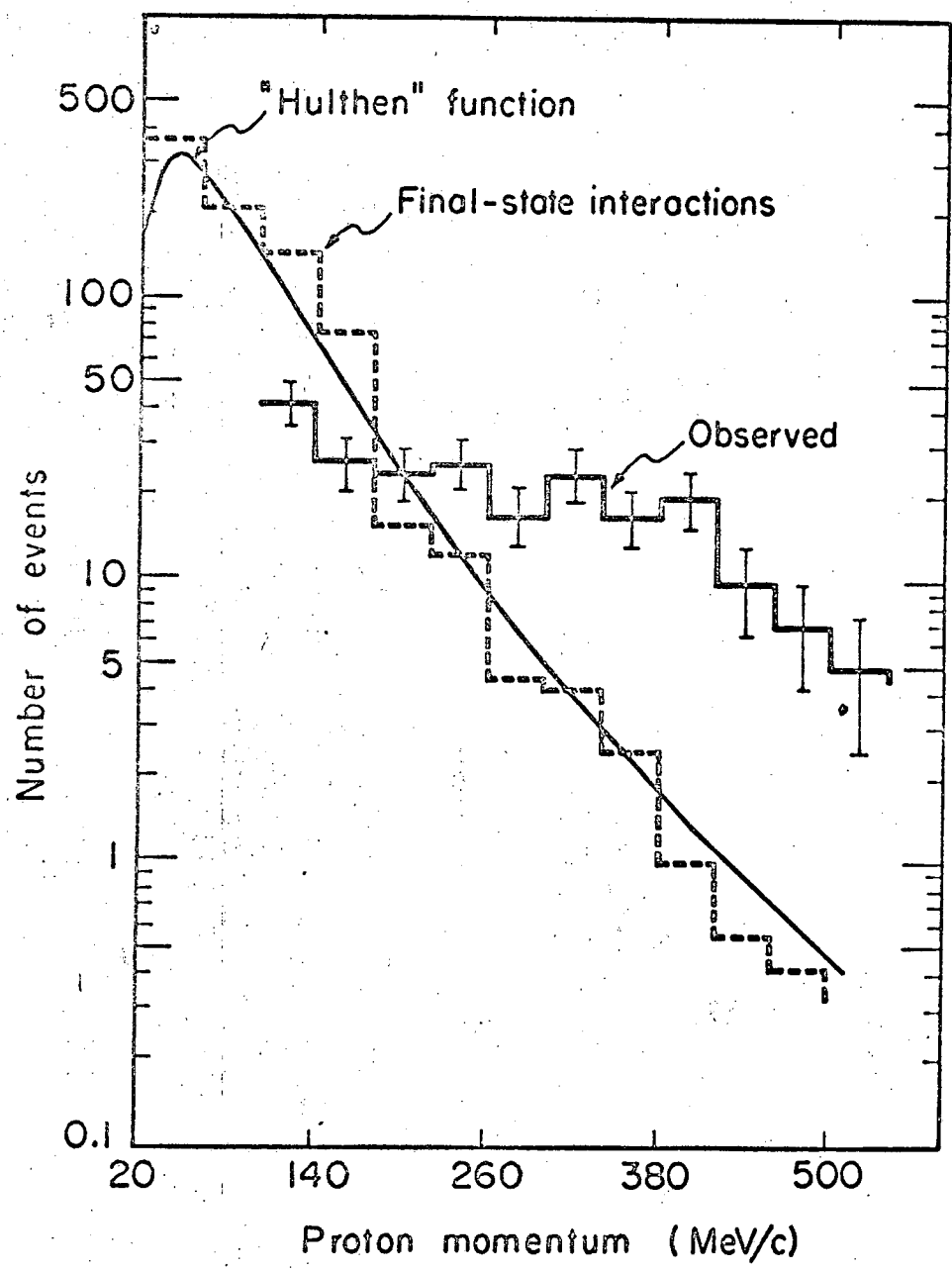


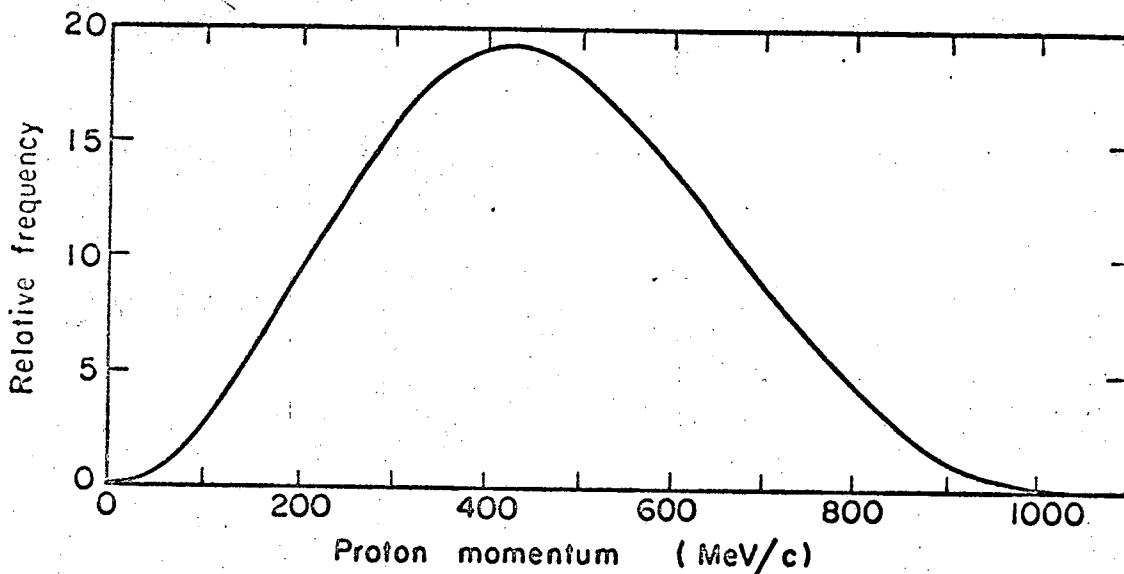
Fig. 17. Observed momentum spectrum of proton spectators in $\bar{p}d$ annihilations into three and five charged pions compared MUB-7716 with a calculated distribution in which the resonant pion-proton interaction in the final state of five pions and a proton was taken into account. The latter is shown in the dotted histogram, a result of a Monte Carlo calculation. For comparison, the "Hulthen" spectrum is shown also.

statistical model for the N* production and assuming isotropic decay for the resulting baryon (Fig. 18). However, agreement with the observed data is poor.

If a significant number of N*'s are produced, then we would expect the π^+p effective mass distribution (Fig. 19b) to peak near the N* mass, 1238 Mev; however, this is not the case. Further, we would expect the shape of the π^-p effective mass distribution (Fig. 19a) to be different from that of the π^+p , since the resonance is in a T = 3/2 state; however, both Figs. 19a and 19b show essentially identical effective mass distributions, both of which peak near 1200 Mev. There is a lack of significant isobar formation in these distributions. Thus, final-state interactions cannot be considered prime contributors to the annihilation dynamics.

3. Three-Body Antiproton Interactions

Griffy and Oakes²⁴ use the spatially symmetric forms, Eq. (27) and Eq. (28), to describe a system of three bodies composed wholly of nucleons (He^3 and H^3). In this experiment the initial state consists of an antiproton, proton and a neutron. It is convenient, but not necessary, to choose spatially symmetric wave forms to discuss a three-body ($\bar{p}np$) system. Perhaps the Irving and the Irving-Gunn functions used to describe the tri-nucleon system are also applicable to the ($\bar{p}np$) system: both have the right asymptotic behavior in configuration space; both have wave forms amenable to analytic discussion. These wave functions are as follows:



MUB-7713

Fig. 18. Calculated momentum spectrum of protons resulting from decay of $N^*(1238)$ produced in the annihilation reaction $\bar{p}d \rightarrow N^* + 4\pi$ proceeding according to the statistical model. The N^* decay is assumed isotropic in the N^* rest system.

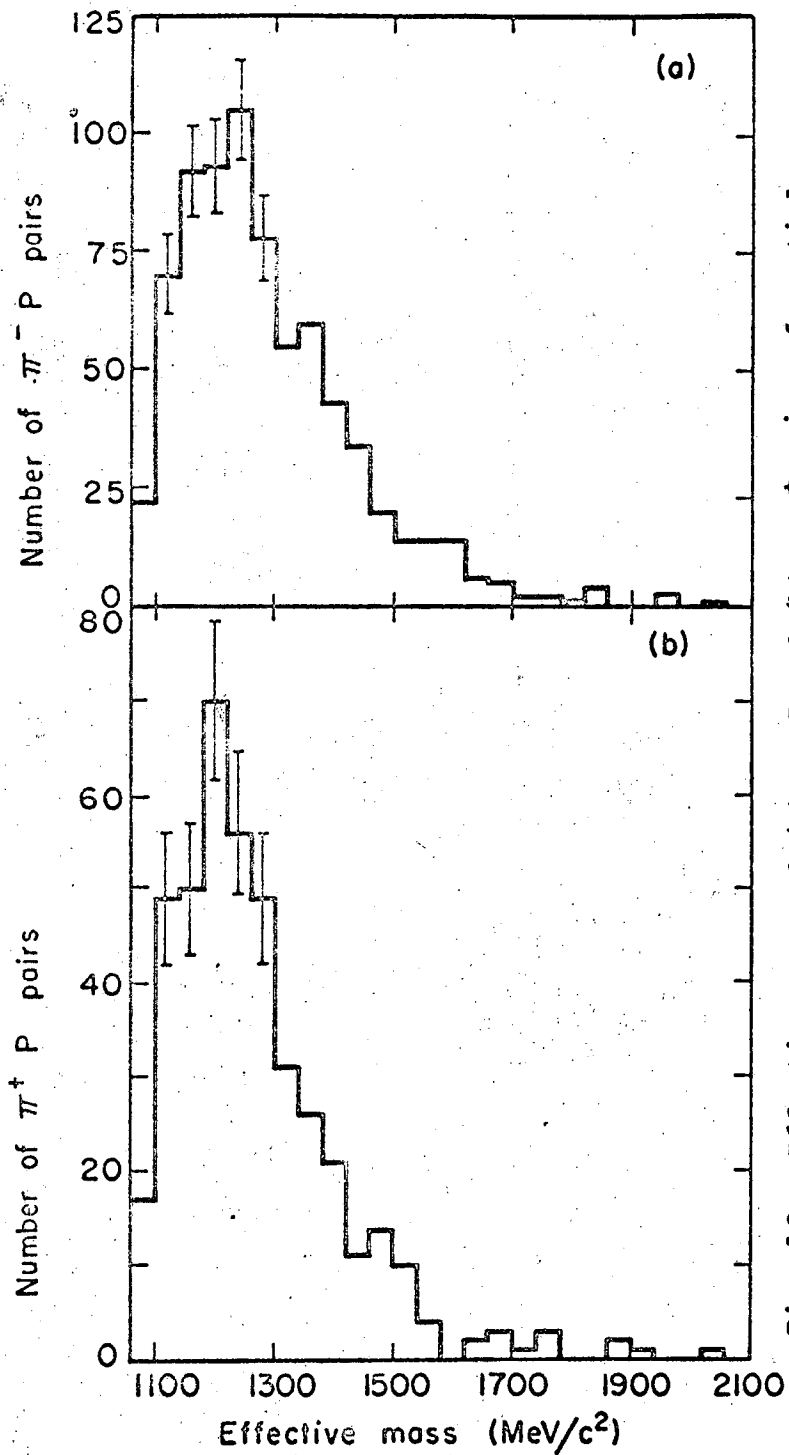


Fig. 19. Effective mass of (a) $p\pi^-$ and (b) $p\pi^+$ pairs of particles produced in the antiproton annihilations on deuterium yielding three and five charged pions in the final state with an identified proton-spectator track.

Irving wave function

$$\begin{aligned} \psi(r_{12}, r_{23}, r_{13}) &= B \exp \left\{ -\frac{\alpha}{2} (r_{12}^2 + r_{23}^2 + r_{13}^2)^{1/2} \right\} \\ &= B \exp \left\{ -\frac{\alpha}{2} \left(2r^2 + \frac{3}{2} \rho^2 \right)^{1/2} \right\} \end{aligned} \quad (27)$$

where $B = \frac{3^{3/4} \alpha^3}{\sqrt{120\pi^5}}$, the normalization constant.

Irving-Gunn wave function

$$\begin{aligned} \psi(r_{12}, r_{23}, r_{13}) &= \frac{C \exp \left\{ -\frac{\alpha}{2} (r_{12}^2 + r_{23}^2 + r_{13}^2)^{1/2} \right\}}{(r_{12}^2 + r_{23}^2 + r_{13}^2)^{1/2}} \\ &= \frac{C \exp \left\{ -\frac{\alpha}{2} \left(2r^2 + \frac{3}{2} \rho^2 \right)^{1/2} \right\}}{\left(2r^2 + \frac{3}{2} \rho^2 \right)^{1/2}} \end{aligned} \quad (28)$$

where $C = \frac{3^{1/4} \alpha^2}{\sqrt{2\pi^3}}$, the normalization constant.

The notation used in Eq. (27) and Eq. (28) is as follows:

$$r_{ij} = r_i - r_j$$

$$r = r_1 - r_2$$

$$\rho = \frac{r_1 + r_2}{2} - r_3$$

The total wave function for the three-body system in the initial state has the form $\Psi(\mathbf{r}) = f(\mathbf{r})\Sigma$, where $f(\mathbf{r}) = \frac{1}{\sqrt{2r^2 + \frac{3}{2}\rho^2}}$. It is symmetric under interchange of any two spatial coordinates of two particles. We will dispense with the spin-isospin (Σ) portion of the wave function because it is not involved in the development of the momentum space eigenfunctions.

The momentum distribution of the proton as given by the Irving and Irving-Gunn function is (see Appendix C):

$$F(Q) = (\text{CONSTANT}) \frac{Q^2}{\left(1 + \frac{Q^2}{2\alpha^2}\right)^{\frac{11}{2} - 2m}} \quad (29)$$

where $m = 0$ for Irving function, and $m = 1$ for Irving-Gunn function and Q is the momentum of the proton.

The phenomenological momentum distribution of the proton developed from the Irving-Gunn wave function for $\alpha = 152 \text{ Mev}^{24}$ appropriate for the three nucleon system, is shown in Fig. 20; the corresponding distribution for the Irving function for an $\alpha = 250^{24}$ is described in Fig. 21; neither of these values of α produce an acceptable fit to the observed distribution of the recoil proton momentum. However, this is not surprising because the values for α stated above are associated with the three nucleon bound systems, whereas in the present interaction one of the particles is an antinucleon. Consequently, the forces (and thus α) associated with the ($\bar{p}np$) system will differ from that of the bound three nucleons.

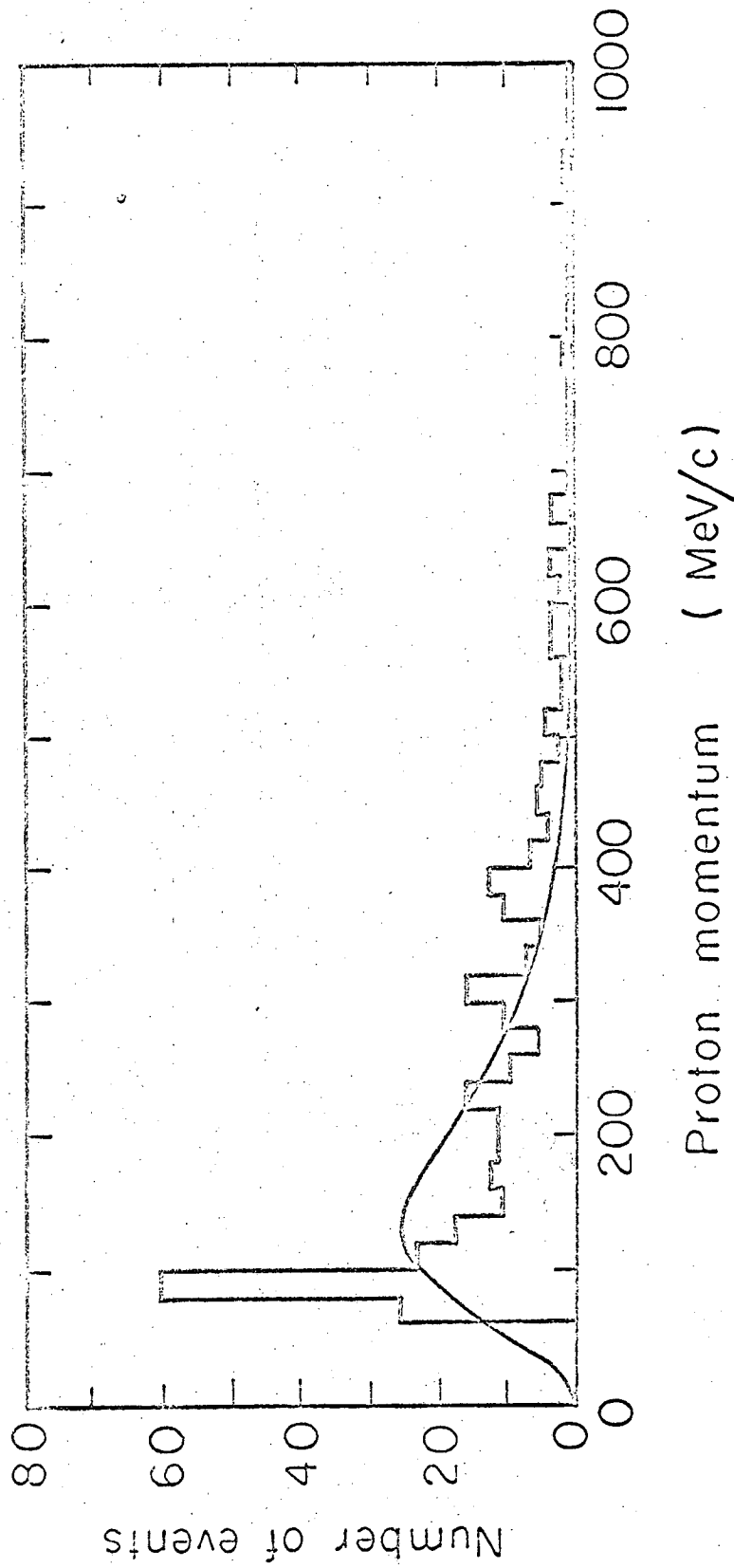


Fig. 20. Momentum distribution of observed, identified proton-spectator tracks resulting from $\bar{p}d$ annihilations into three and five charged pions. The smooth curve is the proton internal-momentum distribution obtained from an Irving-Gunn wave function ($\lambda = 152$ Mev). The smooth curve is normalized to the number of observed protons between 100-1000 Mev/c.

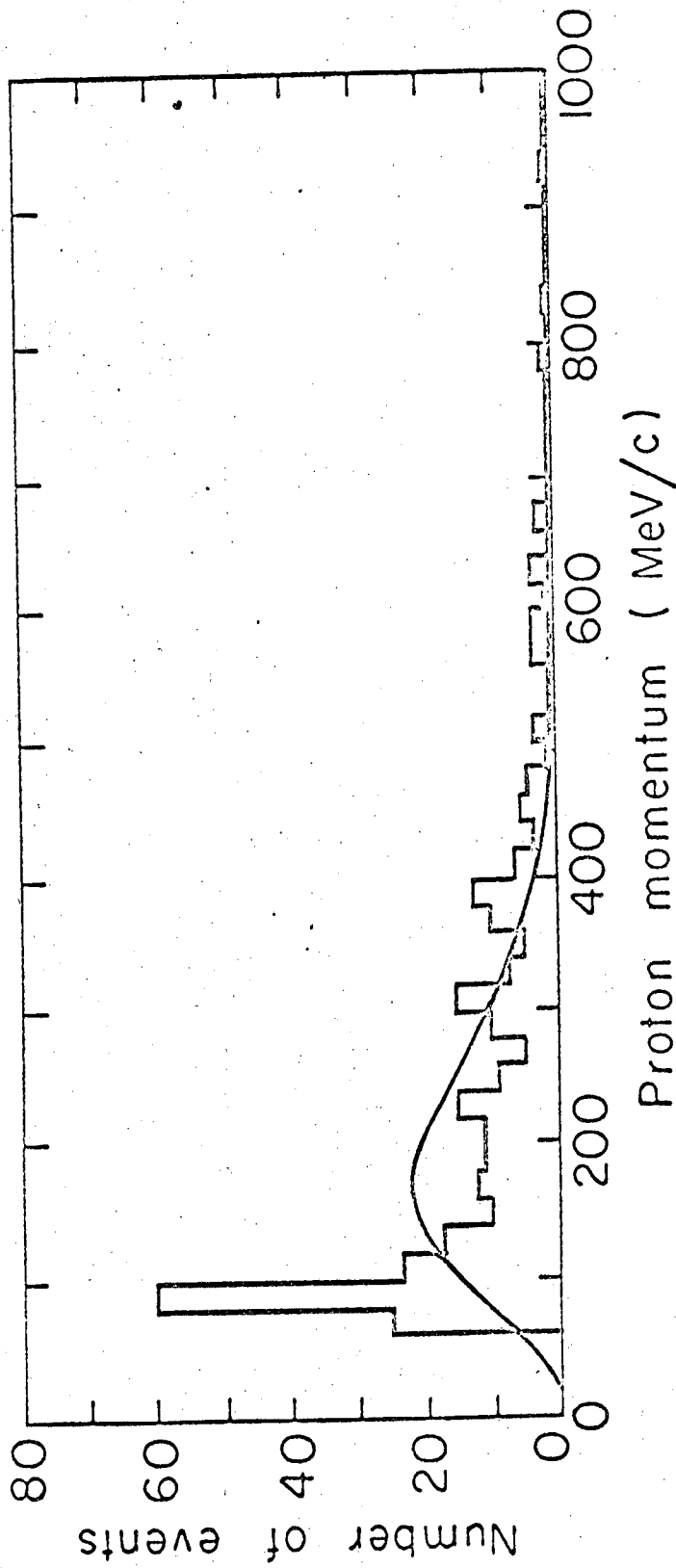


Fig. 21. Momentum distribution of observed, identified proton-spectator tracks resulting from $\bar{p}d$ annihilations into three and five charged pions. The smooth curve is the proton internal-momentum distribution obtained from an Irving wave function ($\alpha = 250$ Mev). The smooth curve is normalized to the number of observed protons between 100-1000 Mev/c.

76-467-1

Choosing a value for $\alpha = 350$ Mev in the Irving form (Fig. 22) and 300 Mev for the Irving-Gunn form (Fig. 23) results in curves that also agree with data in the high momentum region. The area under the Irving and Irving-Gunn curves in Figs. 22 and 23, respectively, are normalized to only those events which had momentum values, for the recoil proton, ranging between 100-1000 Mev/c.

The reasonable behavior in the high momentum region, shown in Figs. 22 and 23, indicates that this portion of the spectrum may be associated with three-body annihilations.

The parameter α is proportional to the \sqrt{E} , where E is the binding energy. The values of the parameter α , as shown in Figs. 22 and 23, result in a system of particles bounded to approximately $1/1.4$ the distance of the triton with a binding energy of about $(1.4)^2$ times as large as the triton. The average value of r , the distance between the proton and neutron, is $\sim 1.5f$, which is equivalent to about 130 Mev/c, the most likely value of the proton.

Apparently at large distances $r > \frac{1}{\alpha}$ (i.e., distances large relative to range of potential) the Irving and Irving-Gunn wave forms with the suggested values for α tend to agree with observation in the high momentum region. If in fact the $\bar{p}d$ bound state constitutes one of the several competing processes in the interaction then the potential associated with this system is $< \frac{1}{\alpha}$.

According to Fig. 15 a peak in the observed momentum distribution is indicated at approximately 300 Mev/c; this is associated with an average separation of $\sim \frac{197 \text{ Mev-Fermi}}{300 \text{ Mev/c}} = 0.66$ fermi for the two nucleons. If the antiproton interacting with the deuteron compacts

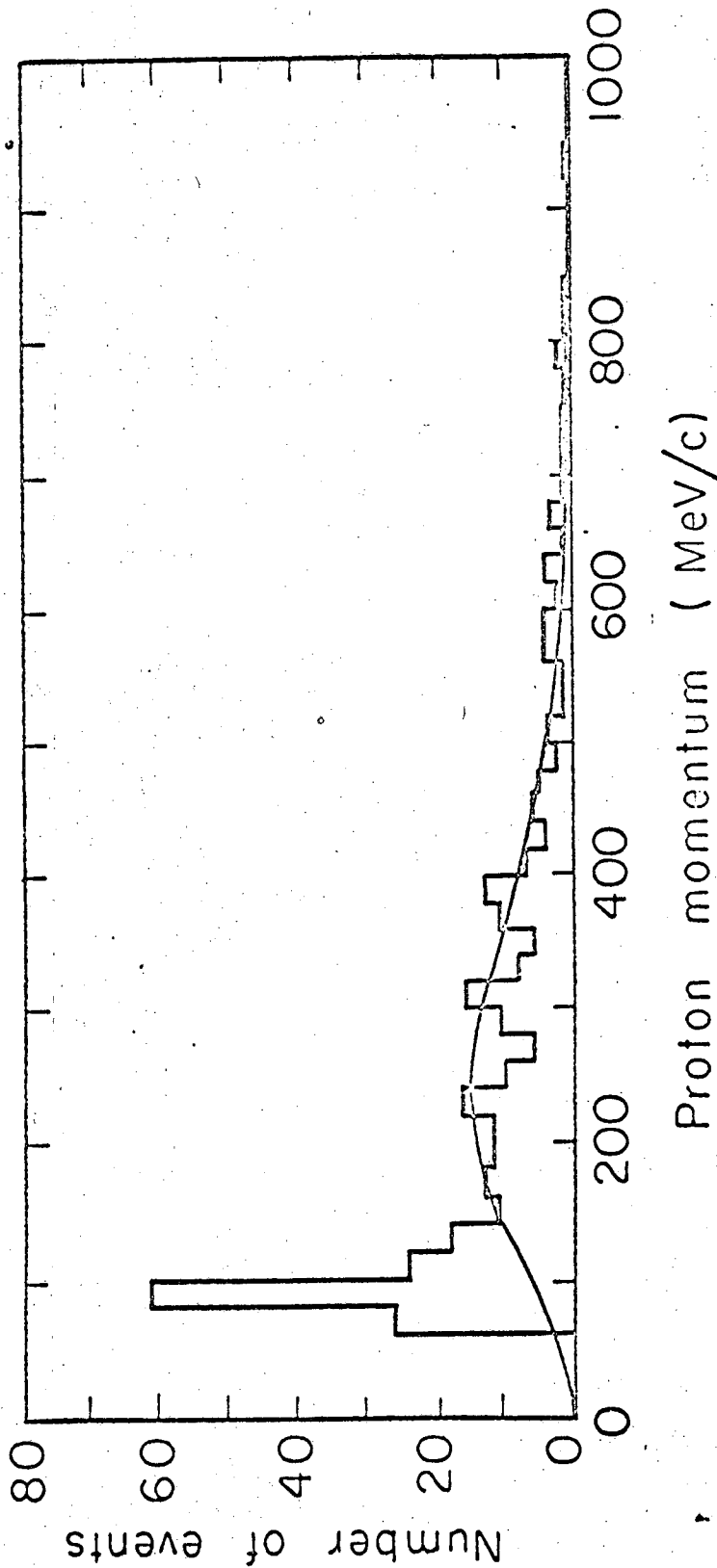


Fig. 22. Momentum distribution of observed, identified proton-spectator tracks resulting from $\bar{p}d$ annihilations into three and five charged pions. The smooth curve is the proton internal-momentum distribution obtained from an Irving wave function ($\alpha = 350$ Mev). The smooth curve is normalized to the number of observed protons between 100-1000 Mev/c.

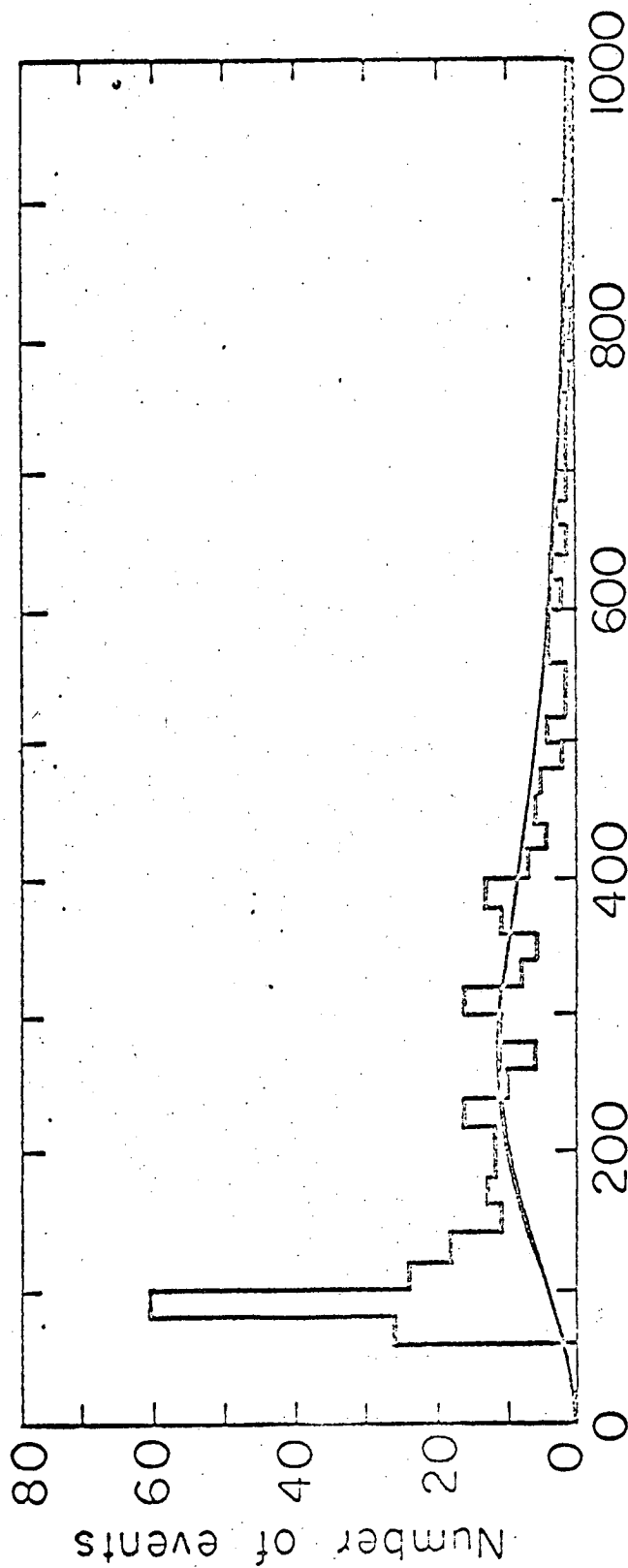


Fig. 23. Momentum distribution of observed, identified proton-spectator tracks resulting from $\bar{p}d$ annihilations into three and five charged pions. The smooth curve is the proton internal-momentum distribution obtained from an Irving-Gunn wave function ($\alpha = 300$ Mev). The smooth curve is normalized to the number of observed protons between 100-1000 Mev/c.



the deuteron, such that the distance separating the deuteron's composite particles is in the neighborhood of $0.66f$, then proton momenta in the range of $300 \text{ Mev}/c$ can be expected.

That portion of the proton momentum distribution spectrum which is not related to two-body annihilations may not be attributed directly to three-body annihilations, because this latter type of interaction requires the production of ~ 8 pions, and very few 7 or 8 pion events were observed. Therefore, it is difficult to state conclusively that the sum of the two- and three-body annihilations are the dominant processes.

The discussion about the detailed shape of the proton spectrum is descriptive only; interaction details for small r are not known. However, the notion that some 20% of the events are produced in some complicated manner, in which the antiproton reacts simultaneously with both particles in the deuteron, cannot be rejected.

We suggest that the observed momentum distribution of the recoil proton may be considered as the sum of three separate functions, resulting from:

1. Two-body annihilations;
2. Three-body annihilations; and
3. Antiproton-neutron bound state.

Using a recoil proton momentum of $300 \text{ Mev}/c$ (which is



consistent with Fig. 15) results in a mass $M=1803$ Mev for the $(\bar{p}n)$ system. Present theory does not preclude the existence of such a state. No estimate of its binding energy or the fraction of annihilation into such a mode is attempted here. The observed data allows for a $(\bar{p}n)$ bound state, but does not require this speculation.

G. Strange Particle Production

Strange particle production from $(\bar{p}d)$ interaction at rest included 76 events with K mesons (see Table III) and 6 with Λ^0 's. They were identified by their decay products or from bubble density estimates. The hyperons which appeared to emanate from the annihilation vertex were all identified on the basis of their decay products, $(\pi^- p)$.

Table III. Observed K meson annihilation product

	K^+	$K^+K_1^0$	K^+K^-	K^-	$K^-K_1^0$	K_1^0	$K_1^0K_1^0$
Neutron annihilation	6	2	3	4	4	9	0
Proton annihilation	10	1	3	13	7	11	3

A momentum distribution was made of all negative K mesons (Fig. 24): 3 were identified from decay products, and 5 interacted with the deuterium medium. Figure 25 shows the corresponding plot of all K^+ tracks, four of which were identified on the basis of decay products. The combined momentum distribution of all charged K mesons is indicated in Fig. 26.

K^0 and \bar{K}^0 decay as K_1^0 , or K_2^0 's with equal with equal probability. The K_1^0 decays into its charged mode ($\pi^+ \pi^-$) and uncharged mode ($\pi^0 \pi^0$), 2/3 and 1/3 of the time, respectively. Therefore, the probability that a K^0 or \bar{K}^0 will decay eventually into a charged (2π) state is 1/3; and of course the probability for entering an unobserved mode is 2/3. The momentum distribution of the K_1^0 's is plotted in Fig. 27.

With the information available in the preceding Table III it is possible, in principle, to determine the detection efficiency for the K mesons and the fractional rates of annihilation into the K^+K^- , K^-K^0 , K^+K^0 and K^0K^0 modes. However, the results are not

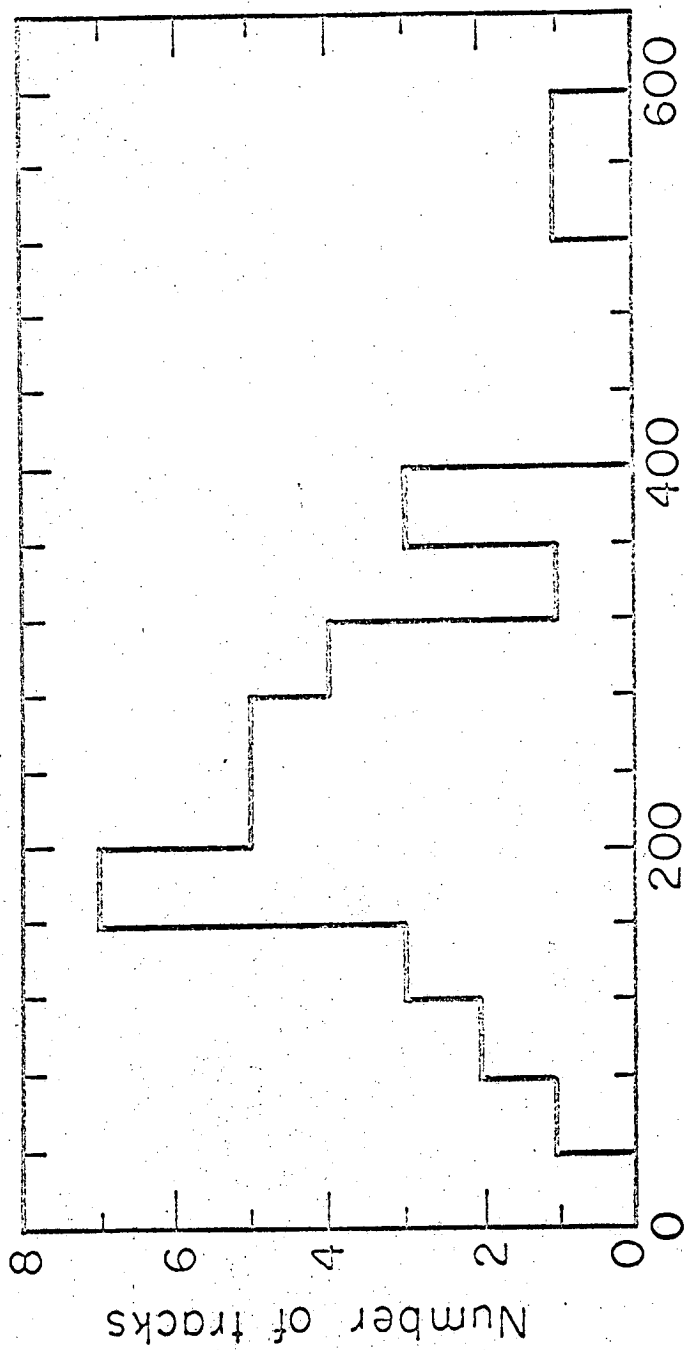


Fig. 24. Momentum distribution of observed K^- tracks resulting from $\bar{p}d$ annihilations.

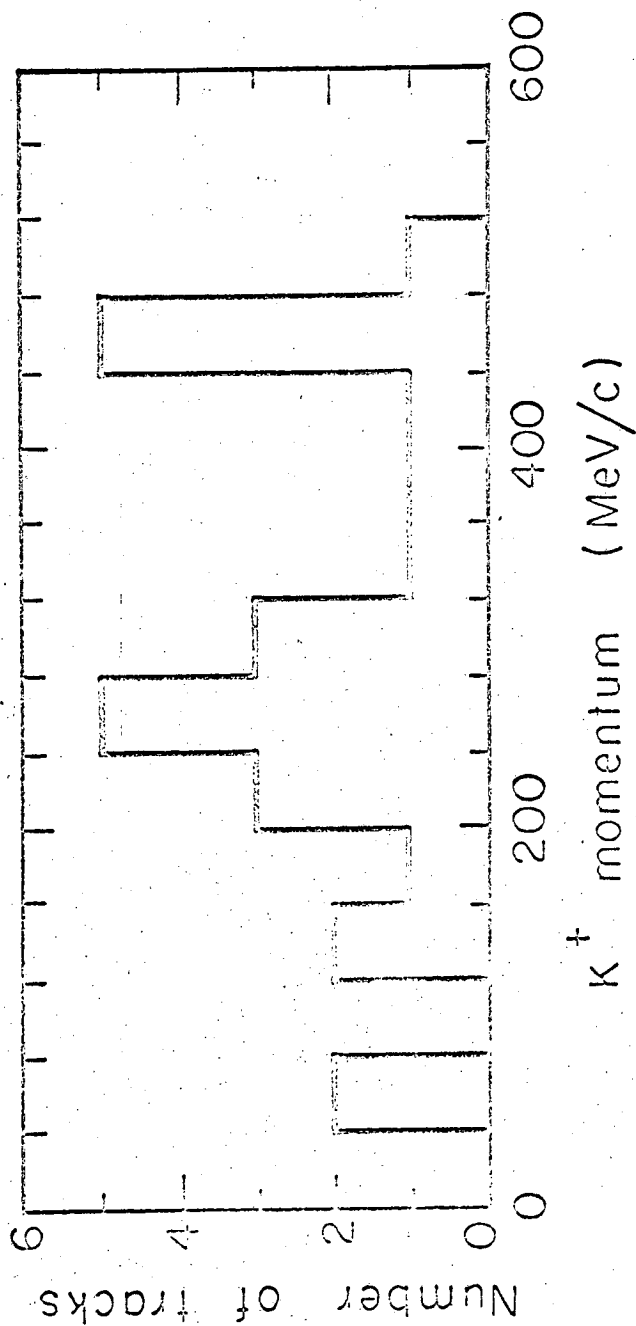


Fig. 25. Momentum distribution of observed K^+ tracks resulting from $\bar{p}d$ annihilations.

46-1171-1

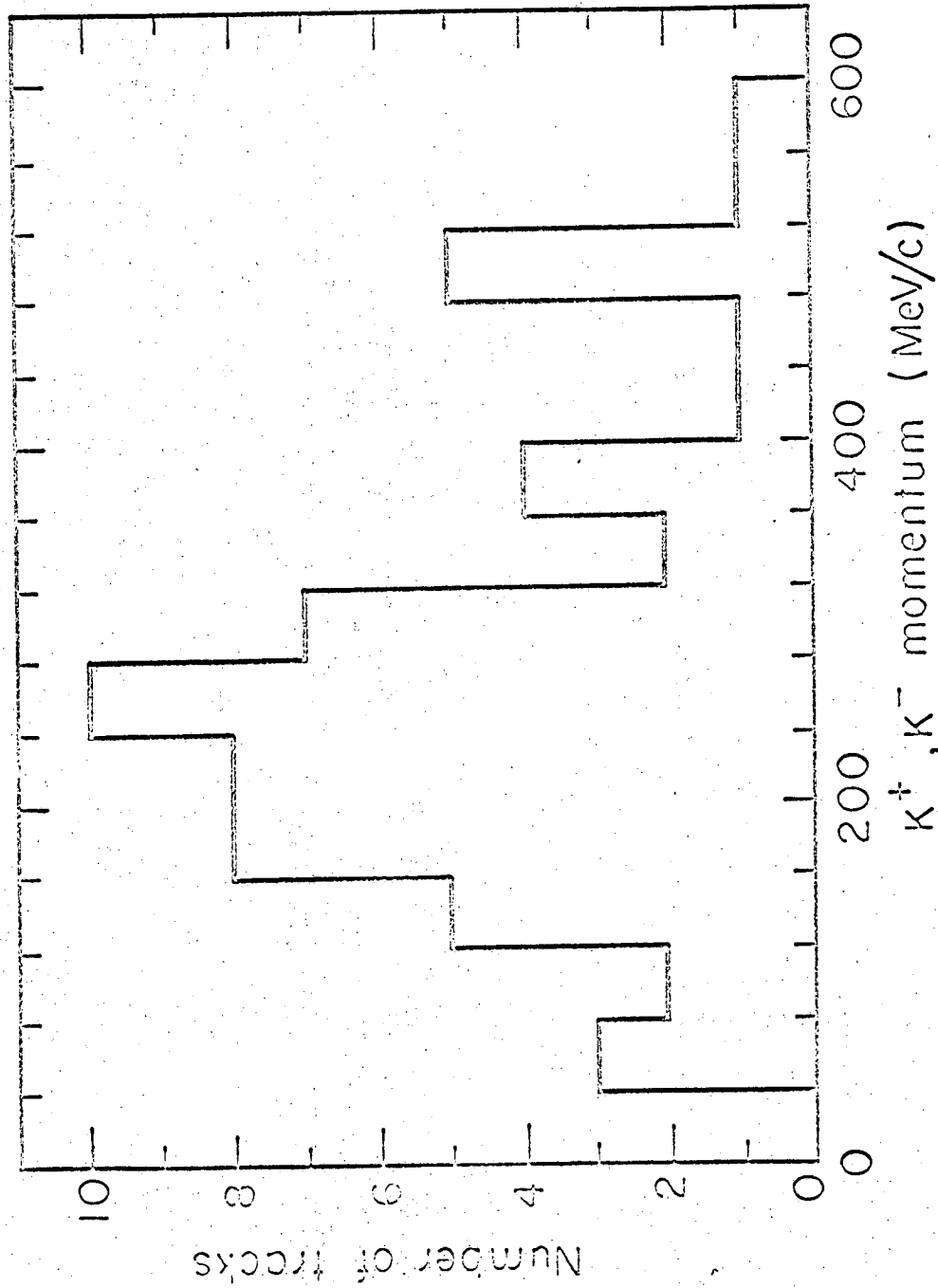


Fig. 26. Combined momentum distribution of observed K^+ , K^- tracks resulting from $\bar{p}d$ annihilations.

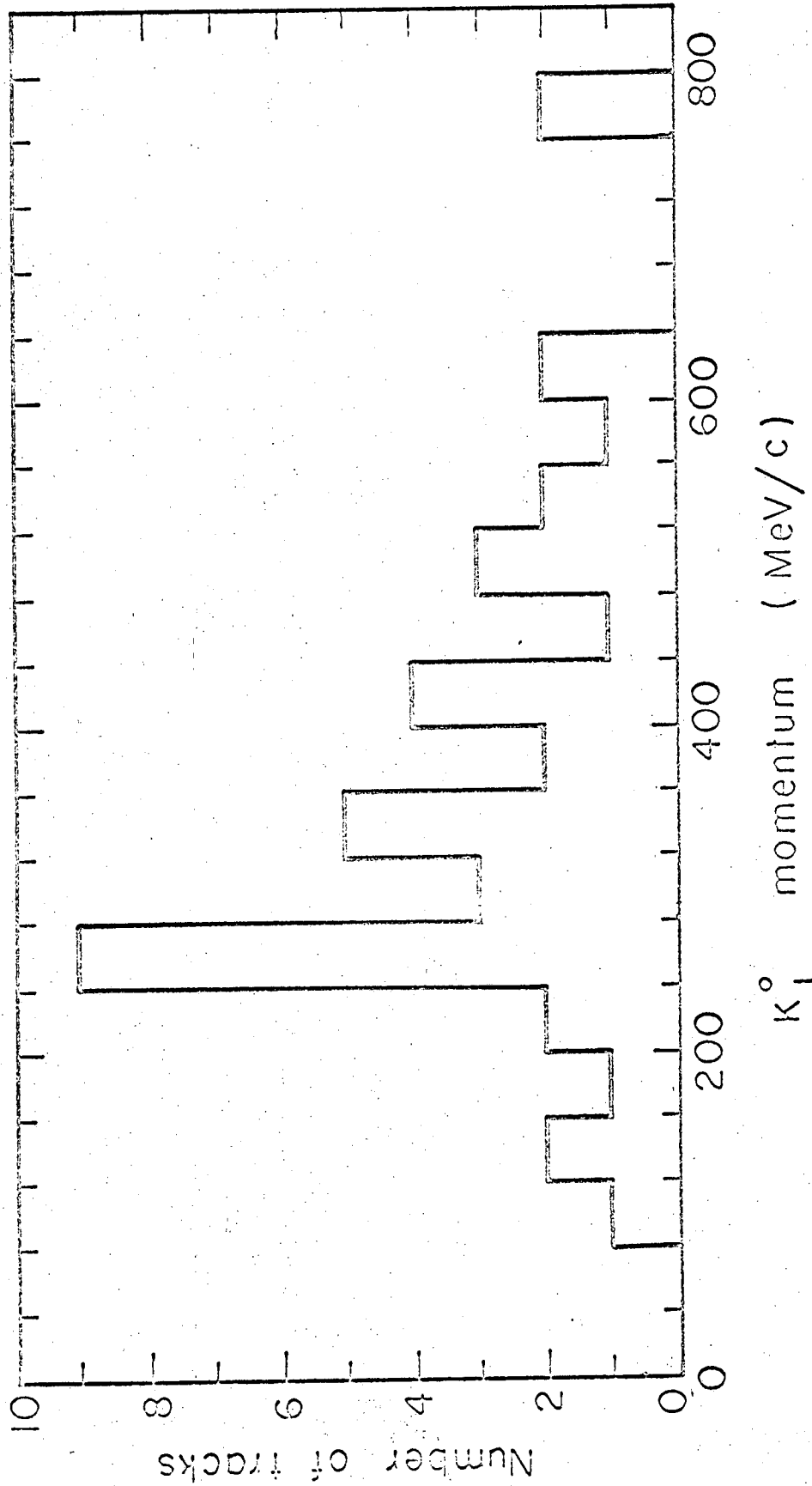


Fig. 27. Momentum distribution of K_1^0 's resulting from $\bar{p}d$ annihilations.

consistent. This is attributed to the small number of strange particle events with its attendant statistical fluctuations.

The estimated value for the K⁺, K⁻'s efficiency is

$\epsilon_{\pm} = 0.5 \pm 0.2$. The stated value for the efficiency is from a combination of effects: of bias in the identification of K mesons, and from the statistical uncertainty. This indicates that about one-half of the K⁺'s and K⁻'s were missed. However, for the neutral K mesons the detection efficiency was assumed to be the product of the probability of decay within the established fiducial volume ($\epsilon_0 = 0.9 \pm 0.1$) and the branching ratio for ($\pi^+\pi^-$) decay, 1/3. We can now determine the fractional rates for annihilation into K mesons from ($\bar{p}d$) interaction at rest. After coupling the scanning efficiencies with the preceding corrections the fractional rates for annihilation into K mesons from ($\bar{p}d$) interaction at rest become:

- R_K (Deuterium) = $.059 \pm .011$
- R_K (Protons) = $.064 \pm .014$
- R_K (Neutrons) = $.053 \pm .013$

These values for the total branching ratio are consistent for branching ratios between .01 and .02, or roughly .015 for the modes K^+K^- , K^+K^0 , K^0K^0 , and K^-K^0 . It is apparent that, within the errors stated, the production rates for K mesons are the same for both neutron and proton annihilations.

ACKNOWLEDGMENTS

It is with pleasure that I acknowledge the aid, advice and continued support of Professor Emilio Segre. I wish to express my appreciation to Professor W.C. Chinowsky for his invaluable guidance, encouragement and interest during the period of this work. I am indebted to Dr. Jonas Schultz for many helpful discussions and assistance in data analysis, and to Professor Kenneth M. Watson for providing the formalism necessary to make the final-state interaction calculation. I thank Dr. Abraham Goldberg and Dr. Robert Oakes for many discussions.

I wish to thank Mr. Robert Kinsey for his assistance during various stages of this analysis. Thanks are also due to Kirmach Natani and Neal Rybicki, who were both helpful in expediting and running programs.

I wish to thank members of the scanning and measuring crew; in particular, George Baker and Gloria Tafraian.

Finally, I thank my wife, Patricia, for her encouragement and understanding during the course of my graduate studies.

This work was done under the auspices of the United States Atomic Energy Commission.

APPENDICES

A. Predictions of the Statistical Model

Fermi²⁵ initially suggested that the phase-space associated with each pion is Ωd^3p , where $\Omega = \lambda \Omega_0$ is the volume of interaction for nucleon-antinucleon, $\Omega_0 = \frac{4}{3} \pi \frac{1}{m_\pi^3}$ and λ is the volume factor. Note throughout this paper $\hbar = c = 1$ and \underline{p} is the momentum of the pion. However, this form of the phase-space for each pion is not Lorentz invariant.

The covariant form $\frac{m_\pi \Omega d^3p}{\omega_\pi}$ for the phase-space

associated with each pion will be used here, where m_π is the mass of the pion and $\omega_\pi = \sqrt{p_\pi^2 + m_\pi^2}$; that is, the total energy of the pion. This form has the property of simplifying the numerical evaluation of phase-space integrals. This expression is plausible on the basis of S-matrix theory. The assumption is made that the matrix element is a constant for the production of n-pions.

The phase-space integral for the production of n-pions with total energy W in the center of mass system is:

$$\left\{ \frac{\Omega}{(2\pi)^3} \right\}^n (2m_\pi)^n F_n(W) \quad (A-1)$$

where $\left\{ \frac{\Omega}{(2\pi)^3} \right\}^m$ is a measure of the probability of finding n -pions in a plane wave momentum eigenstate within the interaction volume. The invariant form of the phase-space integral in the center of mass system at total energy W is defined as follows:⁵

$$F_m(W) = \int \left\{ \prod_{j=1}^m \frac{d^3 p_j}{\omega_{\pi j}} \delta \left[\sum_{j=1}^m p_j \right] \delta \left[W - \sum_{j=1}^m \omega_{\pi j} \right] \right\} \quad (\text{A-2})$$

The transition probability for a state of n -pions into an isotopic-spin state I without the consideration of selection rules is:¹⁶

$$S_m(I) = (\text{CONSTANT}) \frac{G_m(I)}{m!} \left[\frac{2^{m\pi} \Omega}{(2\pi)^3} \right]^m F_m(W). \quad (\text{A-3})$$

The branching ratios for a given number of pions n of total charge Q has been calculated by Pais.¹¹ In the case for which $n = 5$, there are three modes of antiproton-neutron annihilation:

$$\bar{p}n \rightarrow \pi^- + 4\pi^0;$$

$$\bar{p}n \rightarrow \pi^+ + 2\pi^- + 2\pi^0; \quad \text{and}$$

$$\bar{p}n \rightarrow 2\pi^+ + 3\pi^-.$$

The branching ratios are 9/105, 66/105, and 30/105, respectively.

These branching ratios and the $S_n(I)$ values calculated by Desai¹⁶ were used in calculating the fraction of annihilations occurring in each mode for values of n up to seven.

B. Distribution of Momentum Space
Distribution of Hulthén Simulated Hard Core Function

The Hulthén deuteron wave function with a simulated hard core in coordinate space is:

$$\psi(r) = \frac{N}{\sqrt{4\pi}} \left\{ \frac{e^{-\alpha r} - e^{-\beta r}}{r} \right\} f(r), \quad (B-1)$$

where

$$\begin{aligned} f(r) &= 0 & 0 < r < r_c, \\ f(r) &= \sin \frac{\pi}{2} \left(\frac{r - r_c}{d - r_c} \right) & r_c < r < d, \\ f(r) &= 1 & d < r < \infty. \end{aligned} \quad (B-2)$$

The normalization factor N is determined as follows:

$$N^2 = \int_0^\infty f^2(r) dr \left[e^{-2\alpha r} + e^{-2\beta r} - 2e^{-(\alpha+\beta)r} \right]^{-1} \quad (B-3)$$

where $\int f^2(r) dr e^{-\gamma r} = \frac{\pi^2}{2\gamma D^2} \left\{ \frac{e^{-\gamma d} + e^{-\gamma r_c}}{\gamma^2 + \frac{\pi^2}{D^2}} \right\}$, (B-4)

$D = d - r_c$.

Therefore,

$$N^2 = \frac{2D^2}{\pi^2} \left\{ \frac{e^{-2\alpha d} + e^{-2\alpha r_c}}{2\alpha(4\alpha^2 + \frac{\pi^2}{D^2})} + \frac{e^{-2\beta d} + e^{-2\beta r_c}}{2\beta(4\beta^2 + \frac{\pi^2}{D^2})} - \frac{2(e^{-(\alpha+\beta)d} + e^{-(\alpha+\beta)r_c})}{(\alpha+\beta)[(\alpha+\beta)^2 + \frac{\pi^2}{D^2}]} \right\}. \quad (B-5)$$

The Fourier transform is:

$\psi(k) = \frac{1}{(2\pi)^{3/2}} \int dr e^{ikr} \psi(r)$,

$\psi(k) = \frac{N}{\sqrt{2\pi^2} K} \int_0^\infty dr \sin kr f(r) (e^{-\alpha r} - e^{-\beta r})$,

$\psi(k) = \frac{N}{\sqrt{2\pi^2} K} \text{Imaginary} \int f(r) dr e^{ikr} (e^{-\alpha r} - e^{-\beta r})$. (B-6)

And now, substituting for $f(r)$:

$$\psi(K) = \frac{N}{\sqrt{2\pi^2 K}} \operatorname{Imag} \left\{ \int_{r_c}^d dr \sin\left(\frac{\pi(r-r_c)}{D}\right) (e^{-\alpha r} - e^{-\beta r}) e^{iKr} \right. \\ \left. + \int_d^{\infty} dr (e^{-\alpha r} - e^{-\beta r}) e^{iKr} \right\}, \quad (\text{B-7})$$

where

$$\operatorname{Imag} \int_d^{\infty} dr e^{-\gamma r} e^{iKr} = \frac{e^{-\gamma d}}{\gamma^2 + K^2} (K \cos Kd + \gamma \sin Kd), \quad (\text{B-8})$$

$$\operatorname{Imag} \int_{r_c}^d dr e^{-\gamma r} e^{iKr} \sin\left(\frac{\pi(r-r_c)}{D}\right) = \frac{\operatorname{Real Part}}{\lambda} \int_{r_c}^d dr e^{-\gamma r} e^{iKr} \left(e^{i\frac{\pi(r-r_c)}{D}} - e^{-i\frac{\pi(r-r_c)}{D}} \right) \\ = -\frac{1}{\lambda} \frac{1}{(\gamma^2 - K^2 + \frac{\pi^2}{4D^2}) + 4\gamma^2 K^2} \left\{ \frac{\pi}{D} e^{-\gamma r_c} \left[2\gamma K \cos K r_c + (\gamma^2 - K^2 + \frac{\pi^2}{4D^2}) \sin K r_c \right. \right. \\ \left. \left. - 2e^{-\gamma d} \left[\gamma^2 + K^2 + \frac{\pi^2}{4D^2} \right] (\gamma \sin Kd + K \cos Kd) \right\}. \quad (\text{B-9})$$

Incorporate Eqs. (B-8) and (B-9) into (B-7) with the appropriate substitution for γ . Then:

$$\Psi(K) = \frac{N}{\sqrt{2\pi^2}} \left\{ \Phi_\alpha(K) - \Phi_\beta(K) \right\}, \quad (\text{B-10})$$

where

$$\begin{aligned} \Phi_\alpha(K) = e^{-\alpha d} \left(\cos Kd + \frac{\alpha}{K} \sin Kd \right) & \left[\frac{1}{\alpha^2 + K^2} + \right. \\ & \left. \frac{\alpha^2 + K^2 + \frac{\pi^2}{4D^2}}{(\alpha^2 - K^2 + \frac{\pi^2}{4D^2}) + 4\alpha^2 K^2} \right] - \frac{\pi}{2D} e^{-\alpha R_c} \\ & \frac{\left[2\alpha \cos KR_c + \frac{(\alpha^2 - K^2 + \frac{\pi^2}{4D^2}) \sin KR_c}{K} \right]}{\left[\alpha^2 - K^2 + \frac{\pi^2}{4D^2} \right]^2 + 4\alpha^2 K^2} \end{aligned} \quad (\text{B-11})$$

The momentum distribution is:

$$\rho(K) = 4\pi K^2 |\Psi(K)|^2, \quad (\text{B-12})$$

or

$$\rho(k) = \frac{2}{\pi} N^2 k^2 [\phi_\alpha(k) - \phi_\beta(k)]^2. \quad (\text{B-13})$$

C. Derivation of Momentum Space Distribution
of Three-Body Wave Functions

The initial three-body wave function is:²⁴

$$\psi = f(r) \Sigma, \quad (\text{C-1})$$

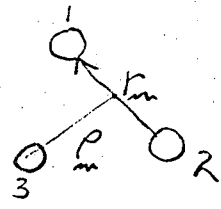
$$\text{where } f(r) = \frac{e^{-\frac{\alpha}{2} \sqrt{2\rho^2 + \frac{3}{2} r^2}}}{(2\rho^2 + \frac{3}{2} r^2)^{m/2}}. \quad (\text{C-2})$$

When $m = 0$ the function has the Irving form, and for $m=1$, the Irving-Gann form. The spatial function $f(r)$ is completely symmetric under the interchange of any pair of nucleons. Σ is the spin-isospin function; it will not be involved in the development of the momentum space eigenfunctions. The notation used is as follows:

- \underline{r}_1 = Position coordinate of particle 1
- \underline{r}_2 = Position coordinate of particle 2
- \underline{r}_3 = Position coordinate of particle 3

- \underline{P}_1 = Momentum of particle 1
- \underline{P}_2 = Momentum of particle 2
- \underline{P}_3 = Momentum of particle 3

All three masses are assumed equal. The vectors $\underline{\rho}$ and \underline{r} are related to the position coordinates of the individual particles in the following way:

$$\underline{\rho} = \frac{\underline{r}_1 + \underline{r}_2}{2} - \underline{r}_3 \quad , \quad \underline{r} = \underline{r}_1 - \underline{r}_2 \quad (C-3)$$


\underline{K} is the vector which describes the momentum of particle 1 with respect to particle 2 and it is conjugate to \underline{r} . \underline{Q} describes the momentum of particle 3 with respect to the center of mass of particles 1 and 2, and it is conjugate to $\underline{\rho}$. These vectors have the following form:

$$\underline{K} = \frac{\underline{P}_1 - \underline{P}_2}{2} \quad ; \quad \underline{Q} = \frac{\underline{P}_1 + \underline{P}_2 - 2 \underline{P}_3}{3} \quad (C-4)$$

According to Griffy and Oakes:²⁴

$$\phi(K, Q) = \int d^3r \int d^3\rho e^{i(Q \cdot \rho + K \cdot r)} f(\rho, r). \quad (C-5)$$

In order to make this six-dimensional integral more manageable we will define

$$\rho = \frac{x}{\sqrt{2}} \quad \text{and} \quad r = \sqrt{\frac{2}{3}} y.$$

As a result, Eq. (C-5) is now:

$$\phi(K, Q) = \frac{1}{\sqrt{3}} \int \frac{d^3x d^3y}{(x^2 + y^2)^{m/2}} e^{-\frac{\alpha}{2} \sqrt{x^2 + y^2}} e^{i\left(\frac{Q}{\sqrt{2}} \cdot x + \sqrt{\frac{2}{3}} K \cdot y\right)} \quad (C-6)$$

With R and L are the six-dimensional vectors:

$$\underset{\sim}{R} = \begin{pmatrix} x_1 \\ x_2 \\ x_3 \\ y_1 \\ y_2 \\ y_3 \end{pmatrix} \quad \underset{\sim}{L} = \begin{pmatrix} \frac{Q_1}{\sqrt{2}} \\ \frac{Q_2}{\sqrt{2}} \\ \frac{Q_3}{\sqrt{2}} \\ \sqrt{\frac{2}{3}} K_1 \\ \sqrt{\frac{2}{3}} K_2 \\ \sqrt{\frac{2}{3}} K_3 \end{pmatrix}$$

$$R^2 = X_1^2 + X_2^2 + X_3^2 + y_1^2 + y_2^2 + y_3^2 = X^2 + y^2,$$

$$L^2 = \frac{Q^2}{2} + \frac{2}{3}K^2.$$

Equation (C-6) can be put into the following form:

$$\Phi(K, Q) = \frac{1}{\sqrt{3}} \int \frac{d^6 R e^{-\frac{\alpha}{2} R} e^{i \frac{L}{m} \cdot R}}{R^m} \quad (C-7)$$

The solution is

$$\Phi(K, Q) = \frac{(\text{CONSTANT})}{\left(1 + \frac{L^2}{\alpha^2}\right)^{\frac{7}{2} - m}} \quad (C-8)$$

$$\Phi(K, Q) = \frac{(\text{constant})}{\left[1 + \frac{\frac{Q^2}{2} + \frac{2}{3}K^2}{\alpha^2}\right]^{\frac{7}{2} - m}} \quad (C-9)$$

The probability of finding a particular set of \underline{K} , \underline{Q} is

$$|\Phi(\underline{K}, \underline{Q})|^2 d^3Q d^3K = \frac{(\text{constant}) d^3Q d^3K}{\left(1 + \frac{Q^2}{2\alpha^2} + \frac{2}{3} \frac{K^2}{\alpha^2}\right)^{7-2m}} \quad (\text{C-10})$$

In the center of mass system

$$\underline{P}_1 + \underline{P}_2 + \underline{P}_3 = 0$$

$$\underline{P}_1 + \underline{P}_2 = -\underline{P}_3 \quad (\text{C-11})$$

We are interested in the momentum distribution of particle 3, the proton.

$$\underline{Q} = \frac{\underline{P}_1 + \underline{P}_2 - 2\underline{P}_3}{3} = -\underline{P}_3 \quad (\text{C-12})$$

define:

$$F(Q^2) = \int Q^2 |\Phi|^2 d^3K d\Omega \quad (\text{C-13})$$

$$F(Q^2) = 4\pi Q^2 \int_0^\infty \frac{d^3K}{\left(1 + \frac{Q^2}{2\alpha^2} + \frac{2}{3} \frac{K^2}{\alpha^2}\right)^{7-2m}} \quad (C-14)$$

Angular integration over K gives another 4π :

$$F(Q^2) = (4\pi)^2 Q^2 \int_0^\infty \frac{K^2 dK}{\left(1 + \frac{Q^2}{2\alpha^2} + \frac{2}{3} \frac{K^2}{\alpha^2}\right)^{7-2m}} \quad (C-15)$$

$$F(Q^2) = (4\pi)^2 Q^2 \int_0^\infty \frac{K^2 dK}{\left(1 + \frac{Q^2}{2\alpha^2}\right)^{7-2m} \left(1 + \frac{\frac{2}{3} \frac{K^2}{\alpha^2}}{1 + \frac{Q^2}{2\alpha^2}}\right)^{7-2m}} \quad (C-16)$$

$$F(Q^2) = \frac{(\text{constant}) Q^2 \left(1 + \frac{Q^2}{2\alpha^2}\right)^{3/2}}{\left(1 + \frac{Q^2}{2\alpha^2}\right)^{7-2m}} \int_0^\infty \frac{x^2 dx}{(1+x^2)^{7-2m}} \quad (C-17)$$

where:

$$K_m = \left(\sqrt{\frac{3}{2}} \alpha \sqrt{1 + \frac{Q^2}{2\alpha^2}} \right) X_m$$

$$dK_m = \left(\sqrt{\frac{3}{2}} \alpha \sqrt{1 + \frac{Q^2}{2\alpha^2}} \right) dX_m \text{ and } X_m^2 = \frac{\frac{2}{3} \frac{K_m^2}{\alpha^2}}{\left(1 + \frac{Q^2}{2\alpha^2}\right)}$$

Note when $K = 0$ $X = 0$
 $K = \infty$ $X = \infty$

$$F(Q^2) = \frac{(\text{constant}) Q^2 \left(1 + \frac{Q^2}{2\alpha^2}\right)^{3/2}}{\left(1 + \frac{Q^2}{2\alpha^2}\right)^{7-2m}} \int_0^{\infty} \frac{X^2 dX}{(1+X^2)^{7-2m}} \quad (\text{C-18})$$

The integral term is constant; therefore:

$$F(Q^2) = \frac{(\text{constant}) Q^2}{\left(1 + \frac{Q^2}{2\alpha^2}\right)^{\frac{11}{2} - 2m}} \quad (\text{C-19})$$

which is the equation plotted in Figs. 20, 21, 22 and 23.

REFERENCES

1. P.A.M. Dirac, Proc. Roy. Soc. (London) A117, 610 (1928); Proc. Roy. Soc. (London) A126, 360 (1929); Proc. Cambridge Phil. Soc. 26, 361 (1930); Proc. Roy. Soc. (London) A133, 60 (1931).
2. E. Segré, O. Chamberlain, C. Wiegand, and T. Ypsilantis, Phys. Rev. 100, 947 (1955).
3. E. Segré, Ann. Rev. of Nuclear Sci. (1958), 8, p. 127.
4. O. Chamberlain, G. Goldhaber, L. Jauneau, T. Kalogeropoulos, E. Segre, and R. Silberberg, The Antiproton-Nucleon Annihilation Process, University of California Radiation Laboratory Report UCRL-8424, 1958.
5. T. Kalogeropoulos, A Study of the Antiproton Annihilation Process in Complex Nuclei (Ph.D Thesis), Lawrence Radiation Laboratory Report UCRL-8677, March 6, 1959.
6. R. Armenteros et al., Proceedings of the International Conference on High Energy Physics (CERN, Geneva, 1962).
7. N. Horwitz, D. Miller, J. Murray and R. Tripp, Phys. Rev. 115, 472 (1959).
8. P. Bastien, O. Dahl, J. Murray, M. Watson, G. Ammar, and P. Schlein, Proc. of the Int. Conf. on Instrumentation for High Energy Physics, Berkeley, 1960 (Interscience Publishers, Inc., New York, 1960), pp. 299-301.

9. W.E. Humphrey, A Description of the PANG Program, in Alvarez Group Memorandum No. 111 and No. 115, Lawrence Radiation Laboratory (unpublished).
10. Arthur H. Rosenfeld and James N. Snyder, *Rev. Sci. Instr.* 33, 181 (1962).
11. A. Pais, *Ann. Phys.* 9, 548 (1960).
12. L. Agnew, Jr., T. Elliott, W.B. Fowler, Richard L. Lander, Wilson M. Powell, Emilio Segre, H. M. Steiner, Howard S. White, Clyde Wiegand, and T. Ypsilantis, *Phys. Rev.* 118, 1371 (1960).
13. G.B. Chadwick, W.T. Davies, M. Derrick, C.J.B. Hawkins, J.H. Mulvey, D. Radojicic, C.A. Wilkinson, M. Cresti, S. Limentani, and R. Santangelo, *Phys. Rev. Letters* 10, No. 2 (Jan. 15, 1963).
14. Ek Spong, A. Frisk, S. Nilsson, and B.E. Ronne, *Nucl. Phys.* 22, 353 (1961).
15. S. Berman and R. Oakes, *Nuovo Cimento* 29, 1329 (1963).
16. Bipin R. Desai, Pion Multiplicity in Nucleon-Antinucleon Annihilation, University of California Radiation Laboratory Report UCRL 9024 Rev., 1960.
17. J.E. Russel and G.L. Shaw, *Phys. Rev. Letters* 4, 369 (1960).
18. Y. Yeivin and A. deShalit, *Nuovo Cimento* 1, 1146 (1955).
19. J. Schultz (Ph.D Thesis), Columbia University, 1962 (unpublished).
20. L. Hulthen and A. Sugawara, Handbuch der Physik (Springer-Verlag, Berlin, 1957), Vol. XXXIV.

21. Kiu S. Suh, American J. of Physics 28 (No. 4), 327 (April, 1960).
22. E. Eriksson, L. Hultén and N. Johansson, Arkiv Fysik 25, 463 (1963).
23. John Raymond Gillespie, Final-State Interactions (Holden-Day, San Francisco, 1964); John Raymond Gillespie, The Effects of Final-State Interactions on Scattering Processes (Ph.D. Thesis), Lawrence Radiation Laboratory Report UCRL-10762, 1963 (unpublished).
24. T.A. Griffy and R.J. Oakes, Phys. Rev. 135, B1161 (1964). This page includes other pertinent references.
25. E. Fermi, Prog. Theoret. Phys. 5 (Japan, 1950), p. 570.

This report was prepared as an account of Government sponsored work. Neither the United States, nor the Commission, nor any person acting on behalf of the Commission:

- A. Makes any warranty or representation, expressed or implied, with respect to the accuracy, completeness, or usefulness of the information contained in this report, or that the use of any information, apparatus, method, or process disclosed in this report may not infringe privately owned rights; or
- B. Assumes any liabilities with respect to the use of, or for damages resulting from the use of any information, apparatus, method, or process disclosed in this report.

As used in the above, "person acting on behalf of the Commission" includes any employee or contractor of the Commission, or employee of such contractor, to the extent that such employee or contractor of the Commission, or employee of such contractor prepares, disseminates, or provides access to, any information pursuant to his employment or contract with the Commission, or his employment with such contractor.

